Foundation scour as a geohazard

John M. Harris, Richard J.S. Whitehouse,
Nicholas S. Tavouktsoglou and Pedro M. Godinho

HR Wallingford, Howbery Park, Wallingford, Oxfordshire OX10 8BA, UK
Corresponding author: John M. Harris, j.harris@hrwallingford.com.

Published in the Journal of Waterway, Port, Coastal, and Ocean Engineering, Volume 145 (6), (November 2019)

Abstract

Carrying out a hazard assessment for offshore structures can entail the consideration of a number of different factors. Scour hazard assessments are routinely undertaken, and scour development at offshore structures should be considered a time-varying process. However, scour may take place within a morphologically dynamic environment, the combination of which will impact on the soil-structure-fluid response. This paper presents the analysis of an unique data set that shows the partial collapse of a scour hole at a large monopile foundation within a morphologically active site. The collapse suggests a slope failure mechanism resulting in the movement of around 450 m3 of material within a period of about 75 minutes. The paper analyses the processes involved regarding formation and development of the collapse.

1. Introduction

Over the last three decades, the ambition to develop offshore renewables resources (wind, tides, waves) has led to specific needs for scour hazard assessment relating to the associated foundation structures and cabling necessary for in-field transmission and power export. This requirement has been led, primarily, by offshore wind developments to date, with the rapid growth in offshore wind generating capacity in European waters. To meet the remaining need will require the construction of thousands of foundations in deeper water depths. This will generate new challenges for construction, operation and maintenance. Increasing the understanding of the possible seabed risks associated with installing foundations on the seabed will help manage costs in the longer term.

Scouring due to waves/currents and backfilling under wave action has been examined in the laboratory (e.g. Whitehouse, 1998; Sumer and Fredsøe, 2002; Sumer et al., 2013) and analysed using simple engineering models (e.g. Harris et al., 2010).

To date very little field data is available to investigate the time-evolution of scour caused by the action of currents and waves and flow-structure-interaction at offshore structures in the short- and long-term as continuous monitoring of the seabed at offshore foundations is not common practice. In order to fully understand the scour development through time there is also a requirement to measure the morphological, hydrodynamic and geotechnical conditions in order to provide the context for any observed change. However, flow-induced scouring of the seabed around the wall of the foundation may not be the only process driving seabed change. Sediment transport on the seabed in the form of bedload transport and bedform migration (Soulsby, 1997) can deliver material into the scour hole and the horseshoe vortices around the pile (Whitehouse, 1998) can locally deepen and hence steepen the toe of the scour hole.

Access to survey data has been granted, which provides evidence of a “collapsing” scour hole at an offshore wind turbine monopile foundation (5.7 m diameter, *D*). The collapse suggests a slope failure mechanism resulting in the movement of about 450 m^3 of material over a period of about 75 minutes. The monopile is located on the side of a large sandbank in a tidally dominant environment in about -10.9 m (LAT – Lowest Astronomical Tide) water depth (Figure 1). The monopile foundation is located in a morphodynamically active region with a tidal range that is macro-tidal (> 4 m) within a large shallow water area comprising an extensive network of flats, banks and channels. The seabed sediments are dominated by sands. Evidence from an adjacent borehole suggests the surface sediments consist of fine to medium sand. Below 5 m there may be thin laminations of soft clay.

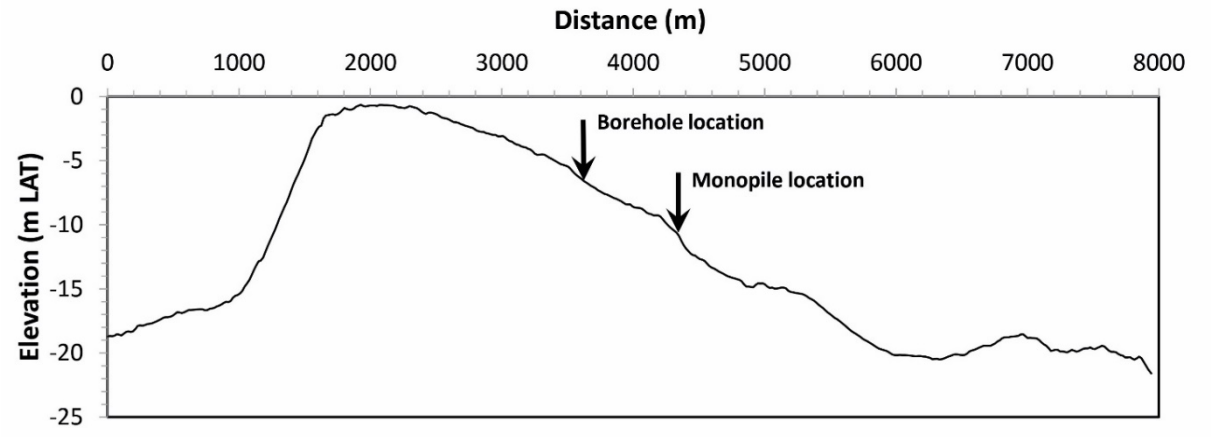

Figure 1: Seabed cross-section (heavily vertically exaggerated) and location of monopile and adjacent borehole.

Pre-installation swath and seismic surveys identified that the monopile was installed on a flat, featureless, sand sheet. This flat bed area is a maximum of 350 m wide and oriented parallel to the bank slope and extends well over 3 km. To both the south-east and north-west of this sheet, the seabed is dominated by asymmetric bedforms (average wavelength, λ = 15 m and 7 m with a height, h = 0.4 m and 0.2 m, respectively). The bedforms indicate a general sediment transport direction to the south-west which will feed sediment across the edge of the scour hole. Bed level change between 2004 and 2010 at this locality is about -1 m, due to long-term migration of the sandbank, resulting in general lowering of the seabed.

Part of the interest in trying to understand the driving mechanism behind the slope failure is the potential hazard it may pose to the operations and maintenance of the offshore foundations and exposure of associated infrastructure such as the inter-array cables. There is also a question as to whether this feature is unique or may occur at other similar locations.

2. Geotechnical and geophysical information

The closest borehole to the monopile foundation was obtained in a water depth of about -6.5 m LAT and achieved a depth of 31.65 m. There was no sample recovery within the first 4 m, although piezocone penetration test data (CPTU) suggest fine and medium sand at 2.0 m depth. Where loss of sample recovery occurred, the boundaries were inferred based on the material recovered from the base of the sample above. Table 1 gives a description of the seabed make up within the first 10 m below the seabed level at the time of survey. The CPTU was carried out in December 2007 and penetrated 21.12 m into the seabed. The CPTU and borehole were not co-located.

The sediment is described as fine to medium sand within the geotechnical samples and this is supported by surficial grab samples collected across the area showing very well to moderately well sorted fine to medium sand, with a median grain diameter (d_{50}) in the range 0.16 mm to 0.36 mm. From the closest borehole to the monopile the sediment at 7 m below seabed is described as brown fine to medium sand with occasional coarse sand sized shell fragments. If it is assumed that the deposits are “draped” over the sandbank, then this data would be representative of sediment close to the base of the scour hole at the monopile. The permeability of the soil is about 5.0 x 10^{-7} m/s with a voids ratio of about 0.43. The bulk density of the sediment is in the range of 2000 to 2200 kg/m^3 and the dry density is about 1900 kg/m^3. The water density at the site is about 1027 kg/m^3 and the sediment particle density is about 2670 kg/m^3.

Table 1: Description of soil strata for nearby borehole.

Depth below seabed (m)	Description of strata
0 – 2	No recovery.
2 – 4	No recovery. CPTU - indicates fine and medium SAND.
4 – 4.1	Brown, fine and medium SAND.
4.1 – 5.27	Brown, fine and medium SAND with some shell fragments. Below 5.00 m; occasional thin laminations of soft grey clay.
5.27 – 6.0	No recovery. CPTU - indicates fine to coarse SAND.
6.0 – 6.5	No recovery (drill out). CPTU - indicates fine to coarse SAND
6.5 – 7.0	No recovery (drill out). CPTU - indicates fine to coarse SAND
7.0 – 7.5	Brown, fine to coarse SAND with many shells and shell fragments (< 3 mm).
7.5 – 8.0	Dark grey, silty SAND with rare shell fragments. SAND is fine and medium. Slight organic odour
8.0 – 9.0	No recovery (drill out). CPTU - indicates fine to medium SAND.
9.0 – 9.1	Brown, fine and medium SAND with occasional shells and shell fragments
9.1 – 10.0	No recovery. CPTU- indicates fine and medium SAND

3. Metocean conditions

The wave regime at the site combines swell waves and more locally-generated wind-waves. The site is open to easterly offshore waves, however, the prevailing direction for locally generated waves is from south-westerly sectors. The sandbanks surrounding the site provide some limited shelter, especially at low water. Around times of low water, the shallow areas of offshore seabed morphology may lead to wave breaking and refraction as waves meet rapid changes in water depth, and wave height to water depth limitations take effect.

Within the study area there is a wave buoy with an Acoustic Doppler Current Profiler (ADCP) attached, measuring waves and current. The wave measurements indicate that during the period over which the slope failure occurred the significant wave height was about 0.3 m with a maximum recorded wave height of 0.67 m (Figure 2).

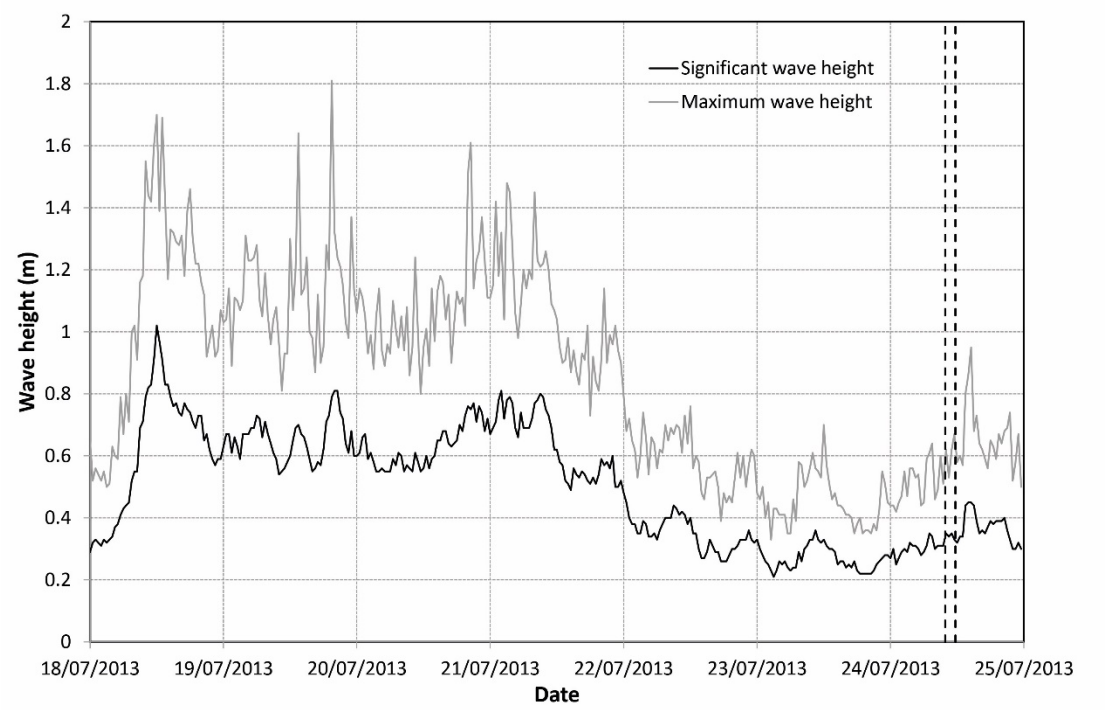

Figure 2: Recorded wave heights at the wave buoy over the period 18 – 25 July 2013. The dashed lines represent the period of the slope failure.

Current speeds are up to about 1.2 m/s and there is a flood-ebb asymmetry in the current towards the south-west which is consistent with the bedform asymmetry. The tidal current data over the period of interest is unreliable due to an instrument error, however, from an earlier study conducted in 2004 another ADCP was placed within about 2.4 km of the monopile foundation. Further, a Delft-3D model of the study area was built and run to simulate the period of deployment of this second ADCP and the results compared with available measured data. The applied model was configured, calibrated and validated to provide a means of linking the ADCP measurements across the site. The model consists of a curvilinear grid with tidal constituents used to provide input conditions along the model boundaries and run with 10 layers through the vertical to provide a 3D description of the study area. Figure 3a shows a comparison of the modelled depth-averaged current

speed with the corresponding ADCP measurements. In general the model gives a reasonable fit to the measured data.

The depth of water at the monopile location means the currents dominate the sediment transport process. Tidal currents are capable of transporting fine sand for about two-thirds of the neap/spring tidal cycle.

Unfortunately, the second ADCP was deployed for a relatively short time, and does not cover the period of interest. However, the data was of sufficient length to allow a harmonic analysis to be undertaken and used to predict the water levels and current speeds at the ADCP location for the period of interest. These results are presented in Figure 3b.

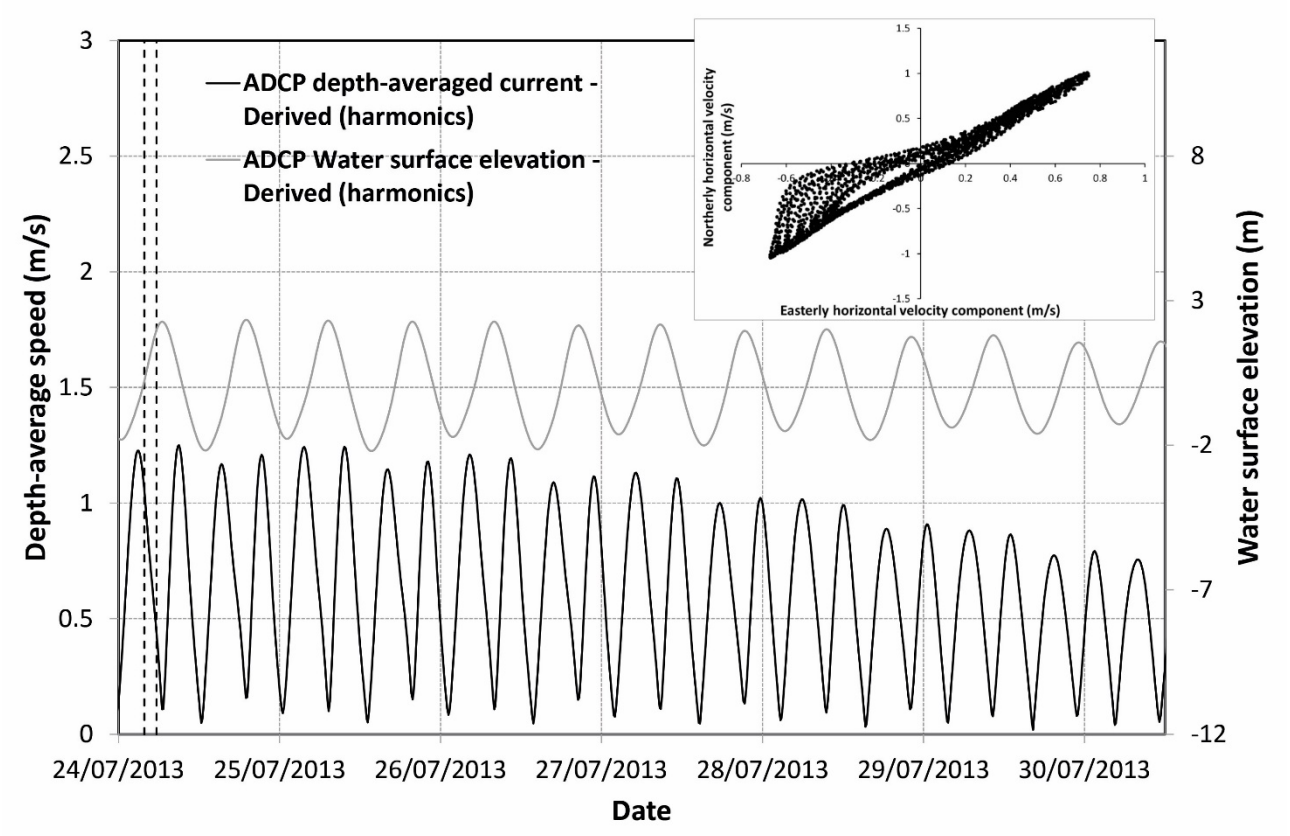

Figure 3: (a) Comparison of depth-average current speed from the short ADCP deployment record together with corresponding model prediction; (b) harmonic prediction of depth-average current speed and water surface elevation at the short deployment ADCP location corresponding to the period of the slope failure during spring tides. Inset shows tidal excursion over predicted period.

Results from the tidal hydrodynamic model of the site indicate the depth-averaged current at the monopile location is of slightly smaller magnitude than that at the ADCP location, although the direction is similar to that at the measurement location.

4. Initial conditions

The monopile was installed in February 2012 with the inter-array cable between the foundation and the adjacent monopile being laid in May 2012. An initial swath bathymetry survey of the site was taken within the month following cable lay and the turbine locality was surveyed again in December 2012 (Figure 4). The May 2012 survey showed that within 3-4 months of installation, a local scour hole had already developed in the seabed, with a maximum depth of -18.1 m LAT, 7 metres lower than the ambient bed level (i.e. local scour depth of 1.2 pile diameters). The scour hole extended 33 m in a south-westerly direction (parallel to the ambient sediment transport direction) and 22 m in a north-easterly direction, with a total surface area of about 2200 m^2. This asymmetry is consistent with both the bedform and tidal flow asymmetry. Typical slope angles within the scour hole were 30° within 7.5 m from the foundation reducing to 10° for the outer part of the hole (Figure 5).

A shaded relief map of the December 2012 survey is shown in Figure 6a.

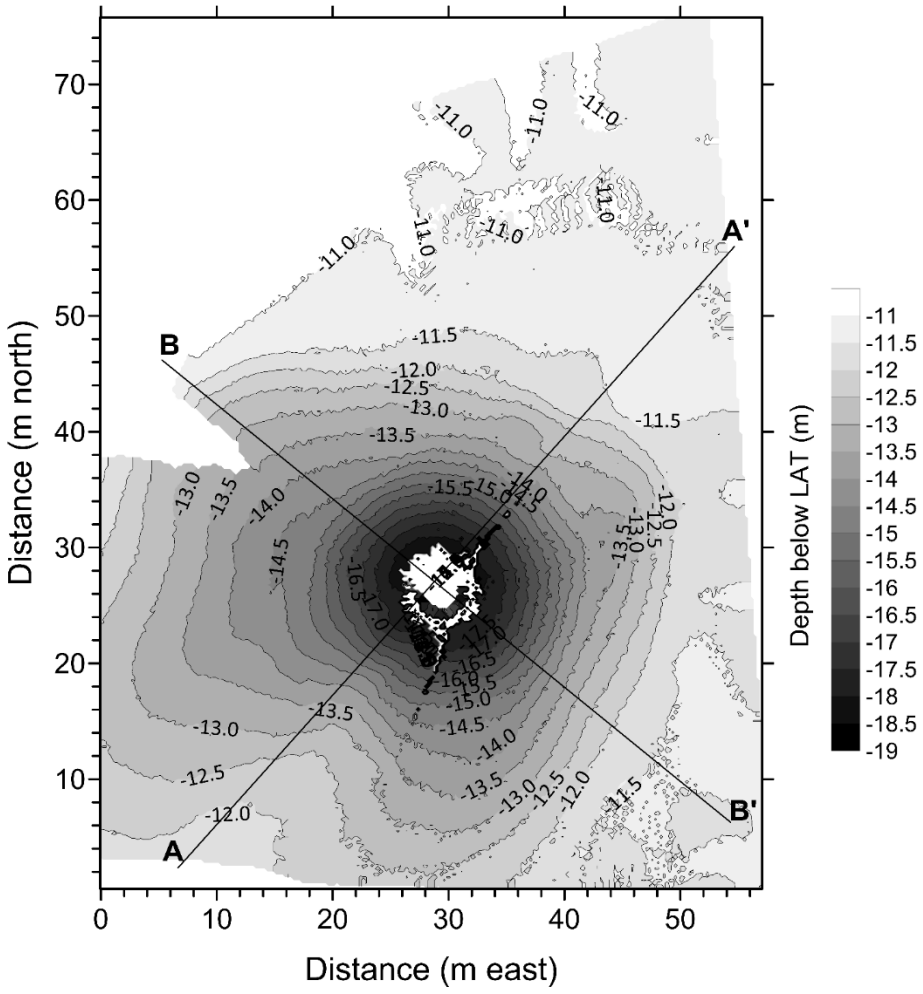

Figure 4: Bathymetric survey at the monopile foundation in December 2012.

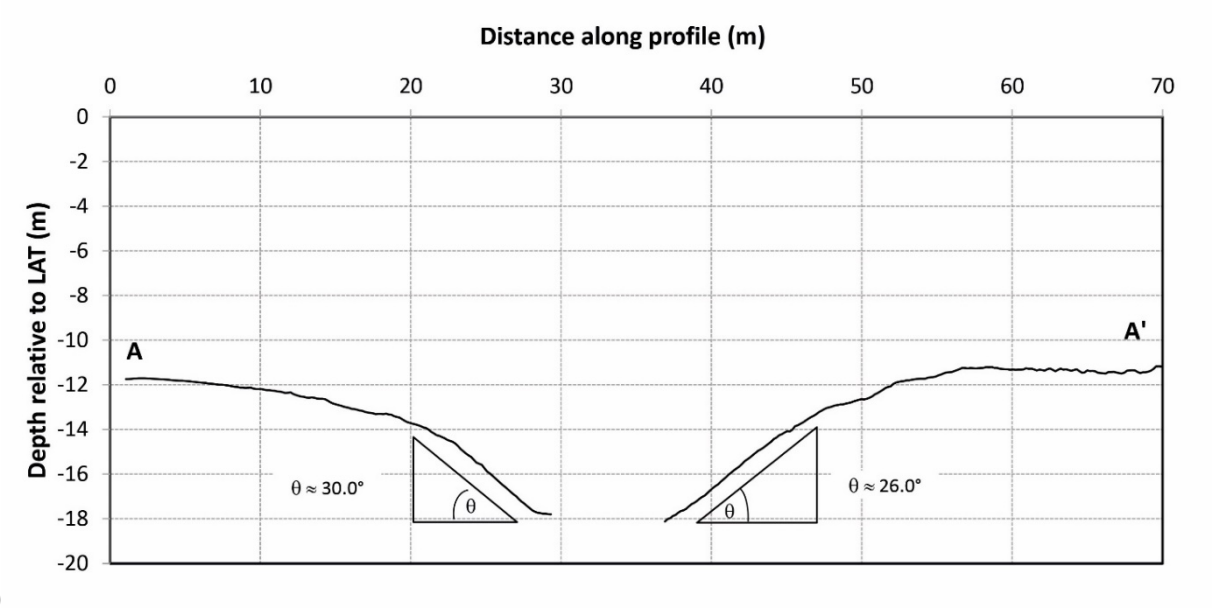

(a)

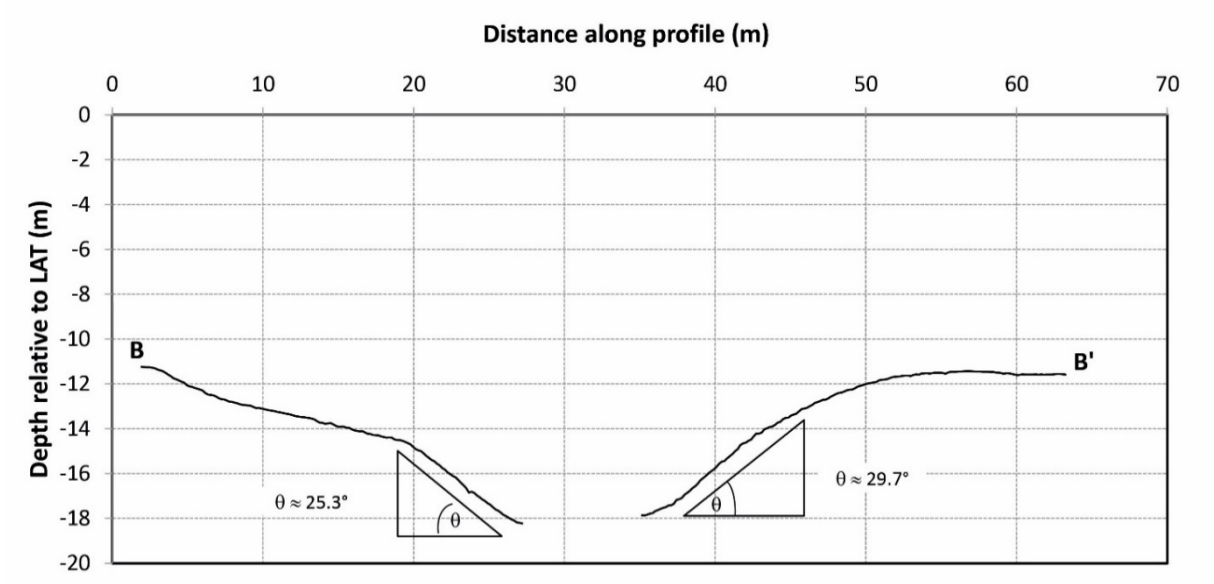

(b)

Figure 5: Cross-sectional profile along lines (a) A-A' and (b) B-B' in December 2012.

5. Slope failure event July 2013

On 24 July 2013 during routine maintenance operations a slope failure event was recorded over a period of 75 mins by the contracted survey vessel. The vessel was undertaking a scour survey of the location at the time and the surveyor observed the event in the echo-sounder return signal. The bathymetric measurements capture the general slope failure over the time frame of the collapse (Figures 6b – 6j). Subsequently, a bathymetric survey was conducted at the monopile foundation 8 months after the observed slope failure event (Figure 6k). This bathymetric survey showed that the scour hole had returned to a shape and depth similar to that observed prior to the failure event, albeit that the scour hole extents had increased by about 10.5 m and the depth of scour had increased by about 0.8 m (Figures 7a and 7b). Given the dynamic nature of the site this is to be expected, although the time required for the scour hole to reassert itself is less certain, but is likely to be about one week, depending on the phase within the spring-neap cycle.

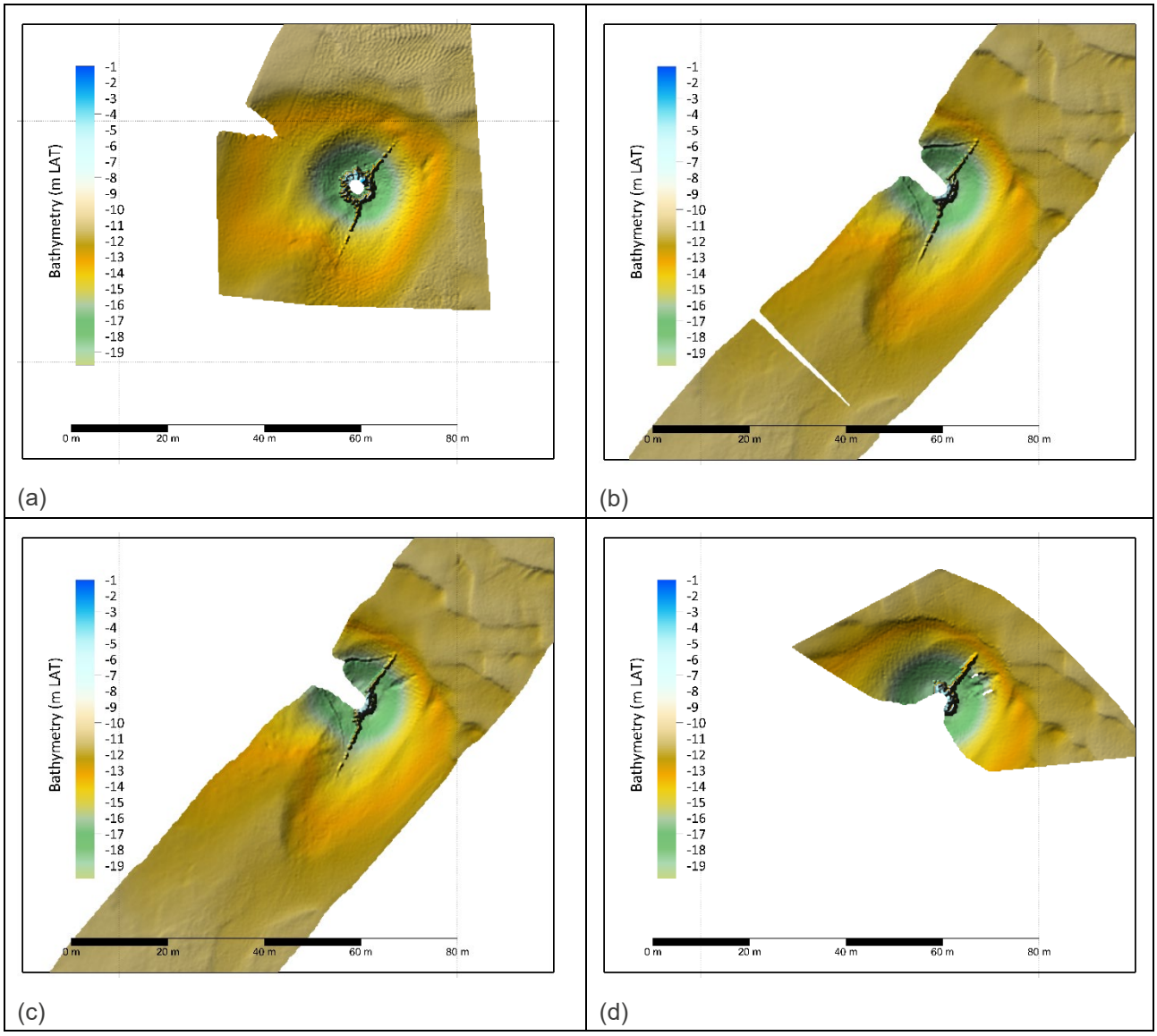

Figure 6: Shaded relief map of bathymetry at the monopile foundation, (a) 17th December 2012; (b) 24th July 2013 about 10:19; (c) 24th July 2013 about 10:26; (d) 24th July 2013 about 10:31.

Continued

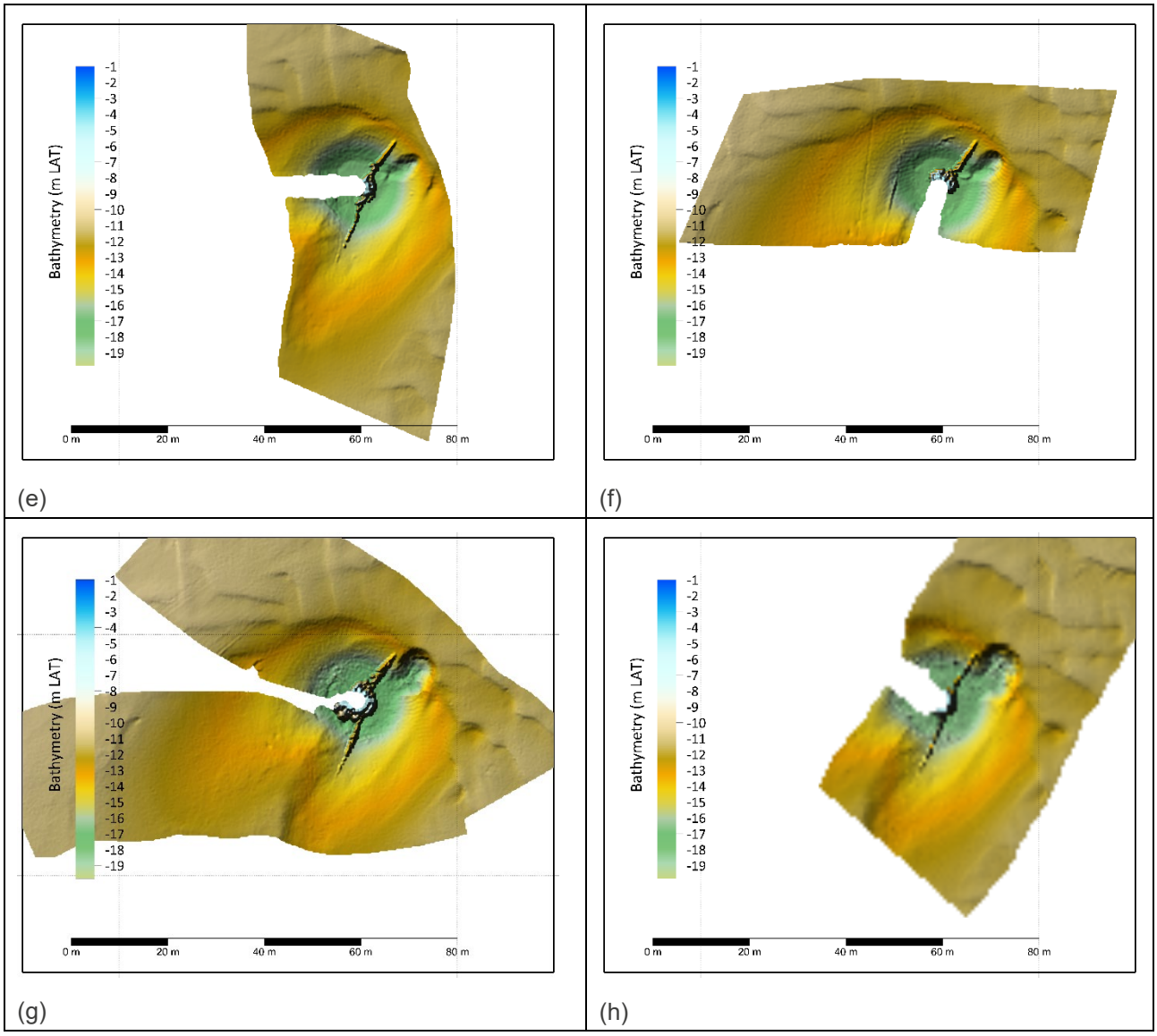

Figure 6: Shaded relief map of bathymetry at the monopile foundation, (e) 24th July 2013 about 10:37; (f) 24th July 2013 about 10:40; (g) 24th July 2013 between 10:47 and 10:50; (h) 24th July 2013 about 10:54.

Continued

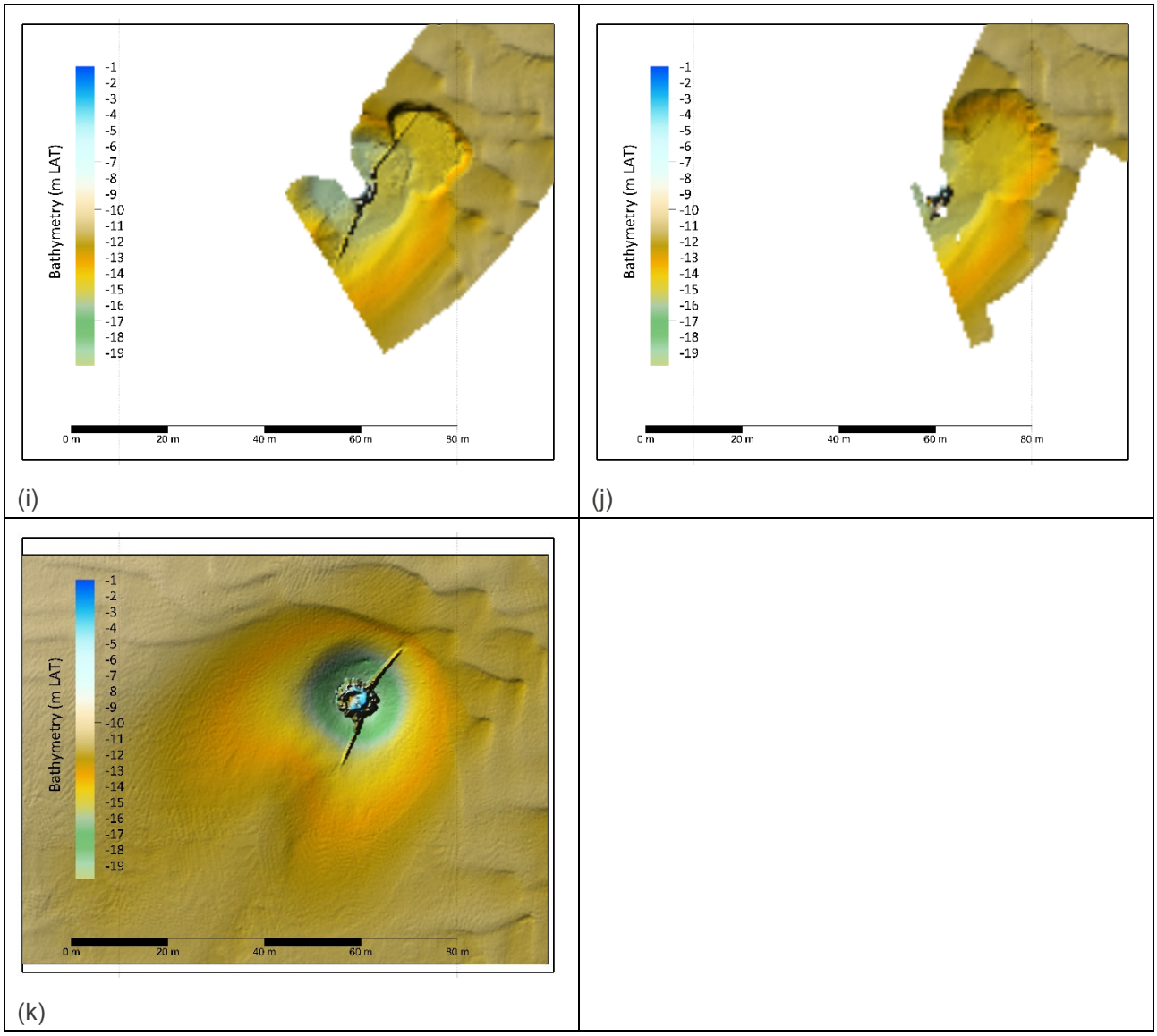

Figure 6: Shaded relief map of bathymetry at the monopile foundation, (i) 24th July 2013 about 11:16; (j) 24th July 2013 about 11:40; (k) 24th March 2014.

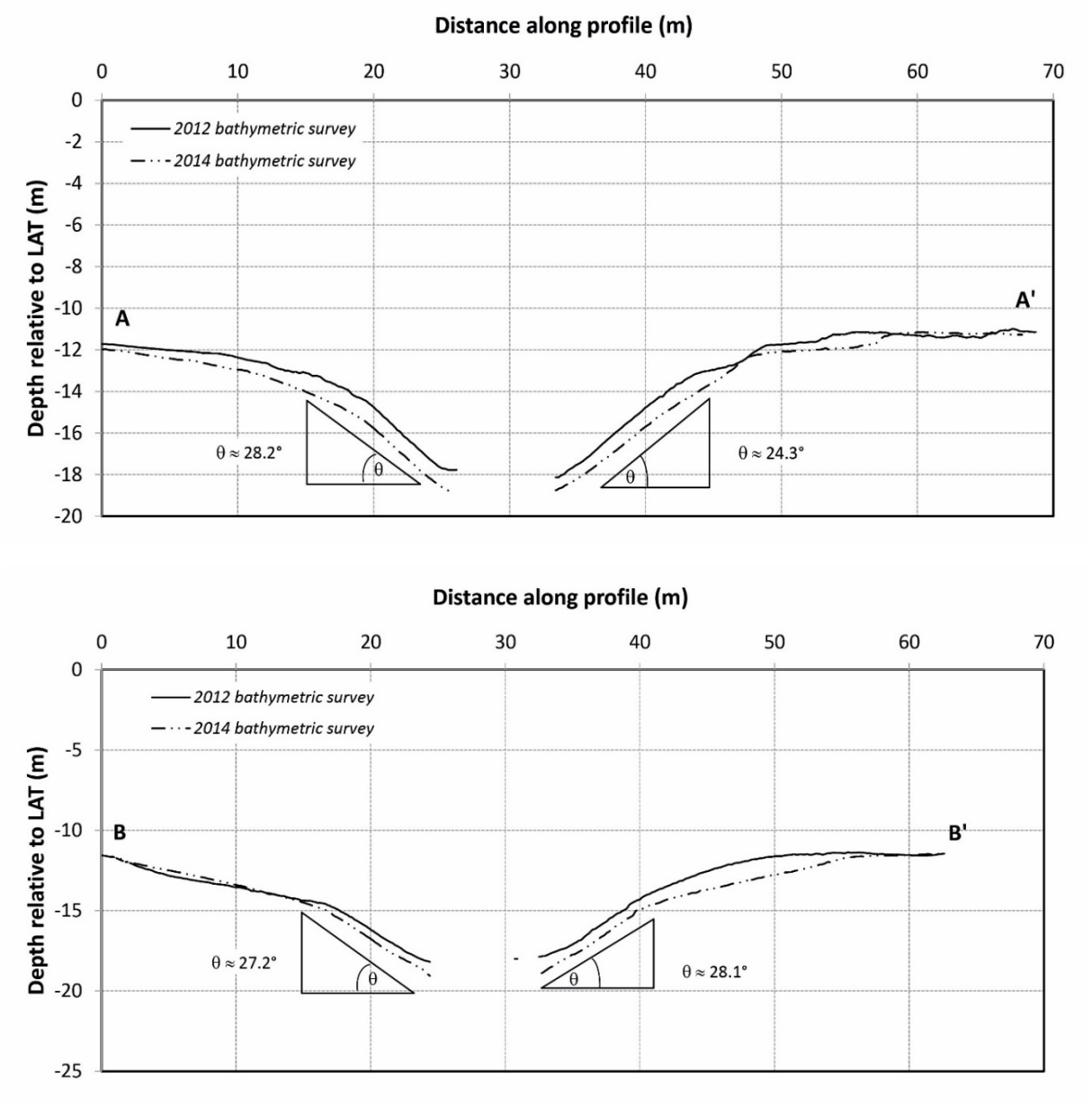

Figure 7: Cross-sectional profiles along lines (a) A-A', (b) and B-B' (Figure 4) for the 2012 and 2014 bathymetric surveys, which are separated by 15 months.

In addition to the 2-dimensional spatial plots, cross-sections were taken through the centre of the monopile at 5° intervals from east to north (east is taken as being at the right hand side of the plot). Figures 8 and 9 show the cross-sections at 20° and 50°, corresponding to the approximate angle along which the slope instability was first observed and principal flow axis and north-easterly array cable alignment, respectively. The cross-sections are presented for the north-east quadrant only.

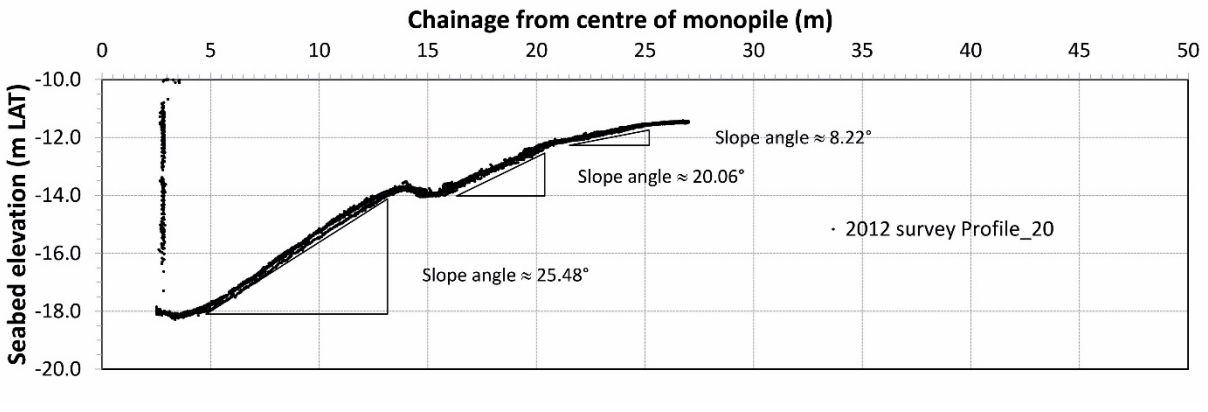

(a)

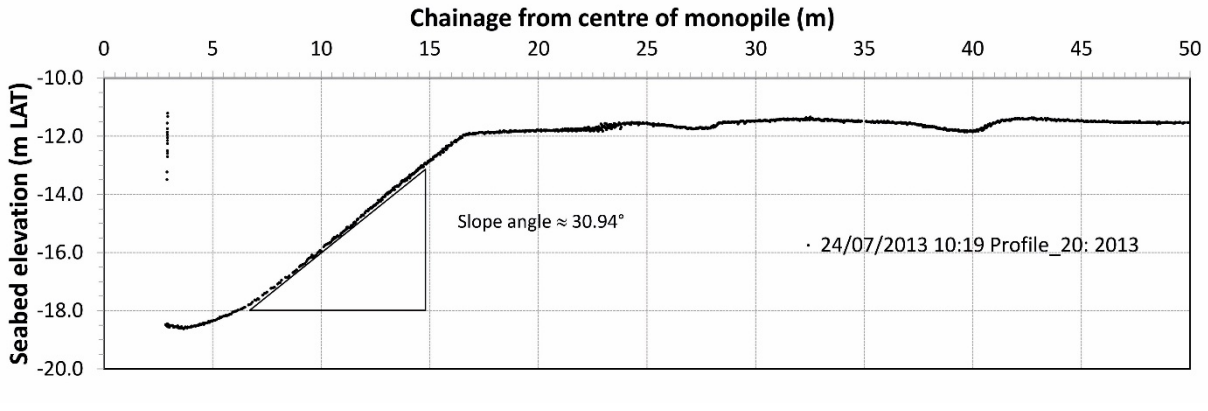

(b)

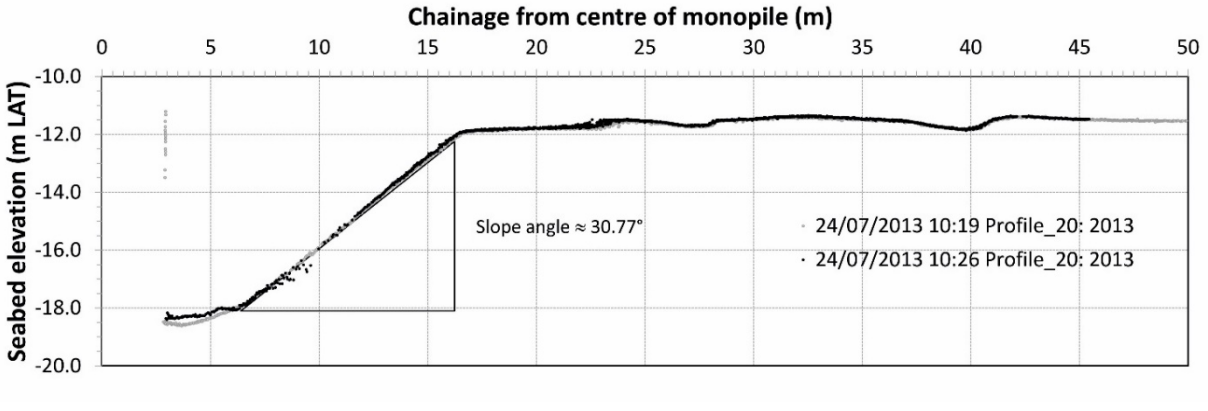

(c)

Figure 8: Cross-sectional profiles along axis of slope failure (20° anticlockwise alignment from east).

Continued

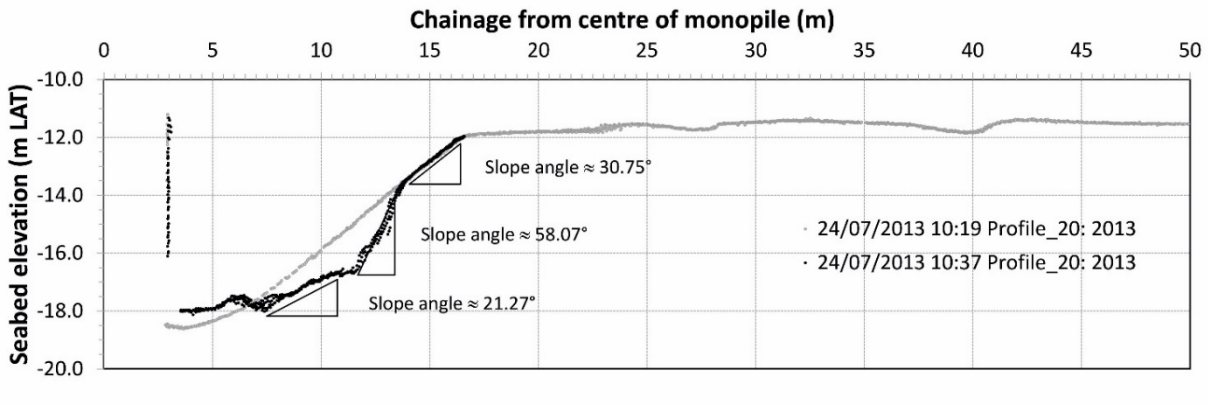

(d)

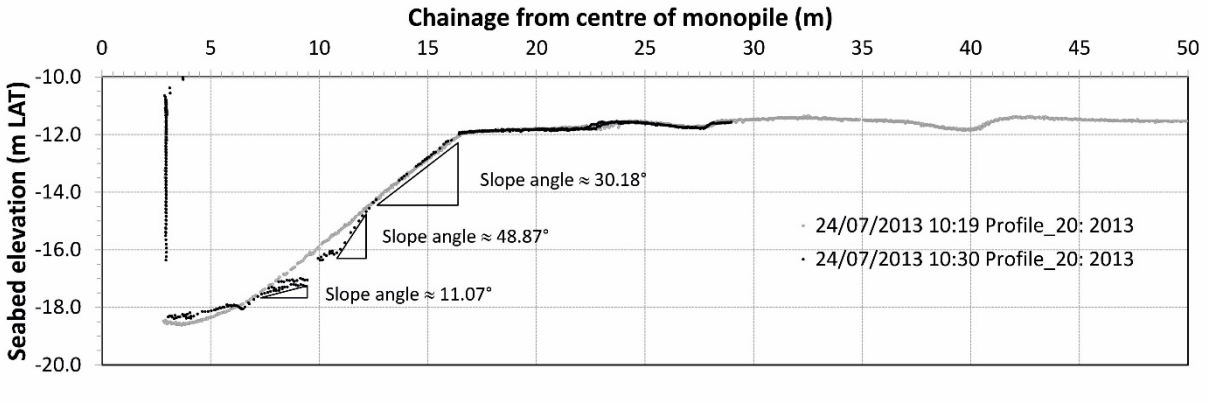

(e)

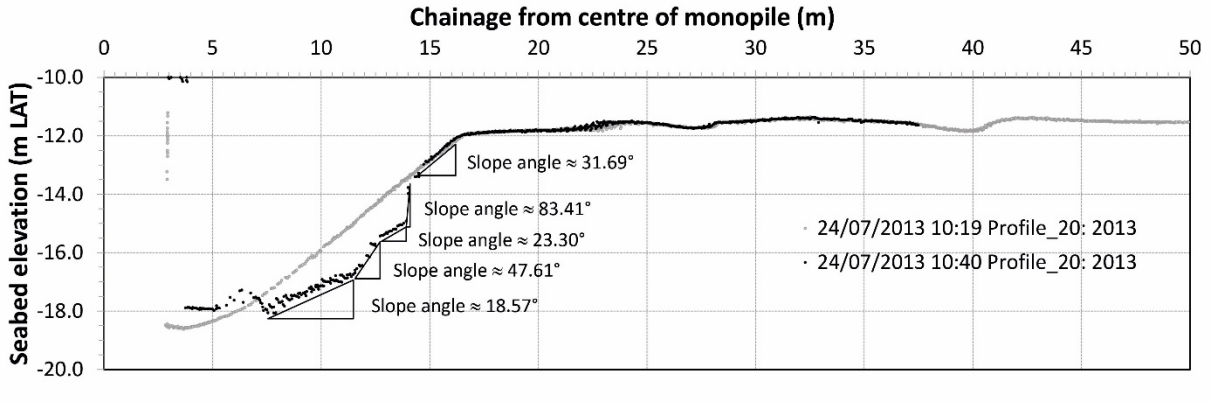

(f)

Figure 8: Cross-sectional profiles along axis of slope failure (20° anticlockwise alignment from east).

Continued

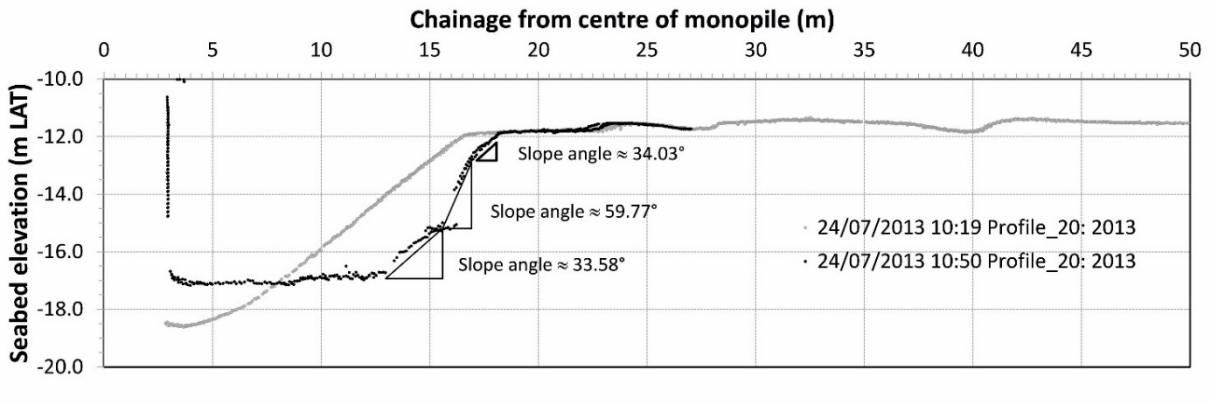

(g)

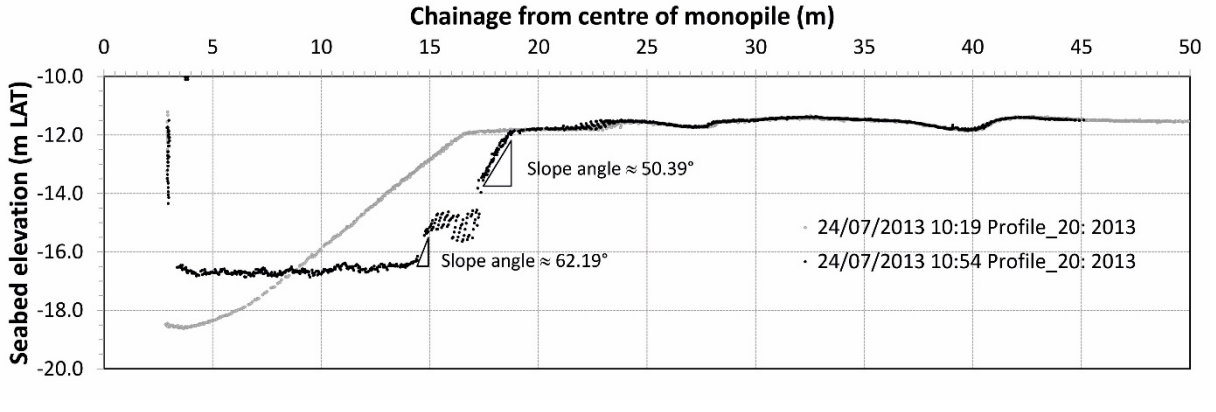

(h)

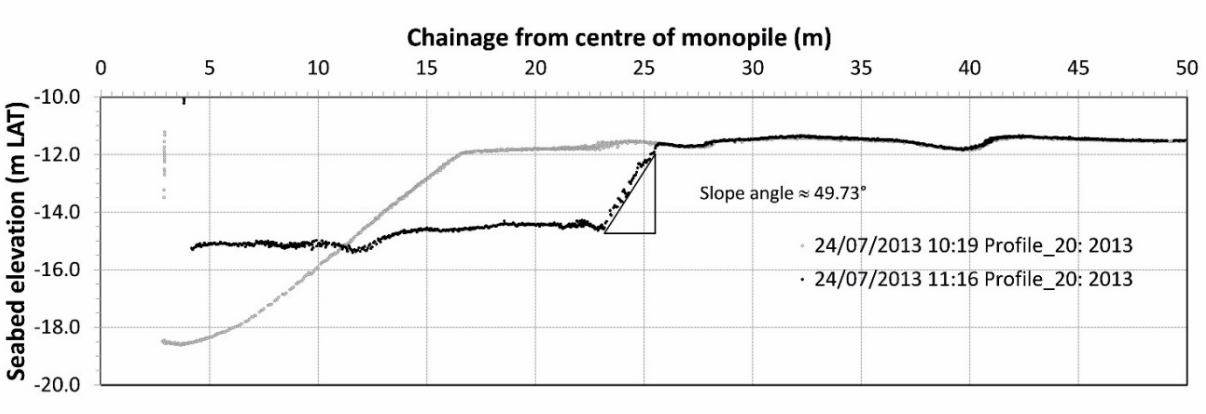

(i)

Figure 8: Cross-sectional profiles along axis of slope failure (20° anticlockwise alignment from east).

Continued

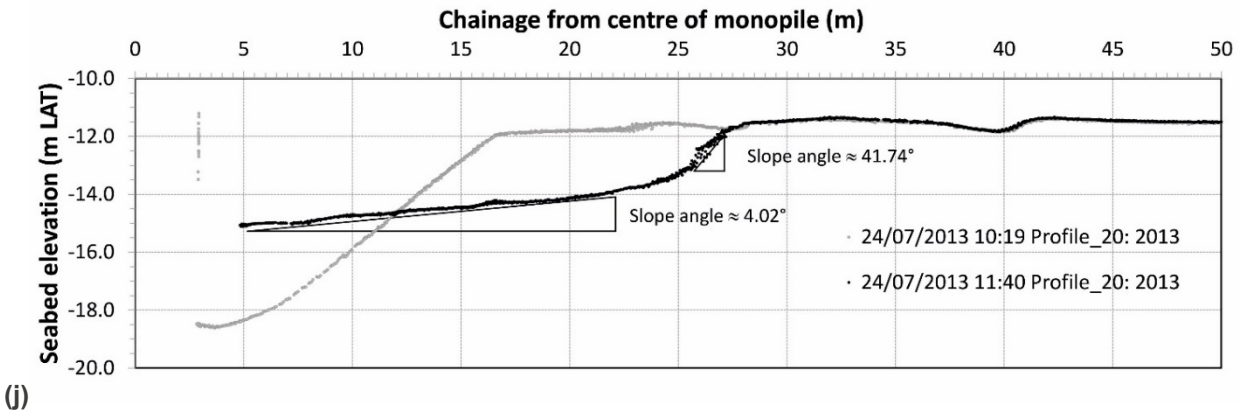

(j)

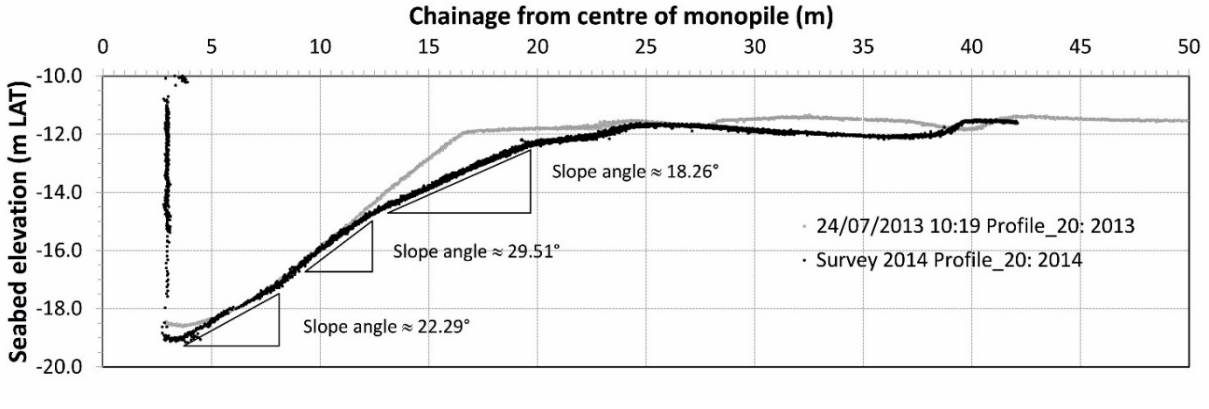

(k)

Figure 8: Cross-sectional profiles along axis of slope failure (20° anticlockwise alignment from east).

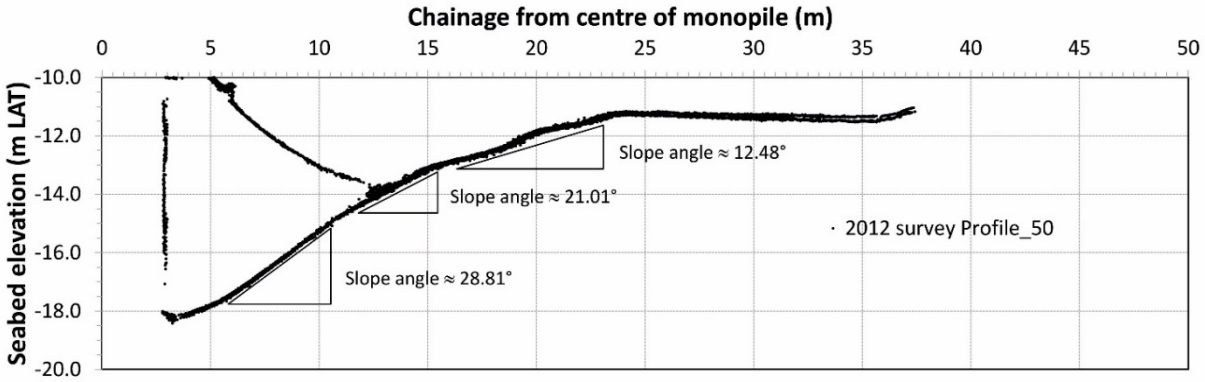

(a)

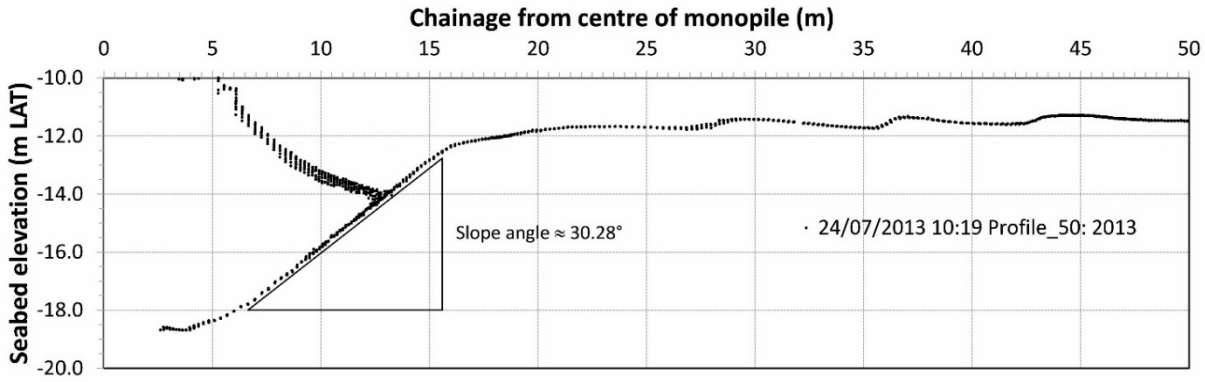

(b)

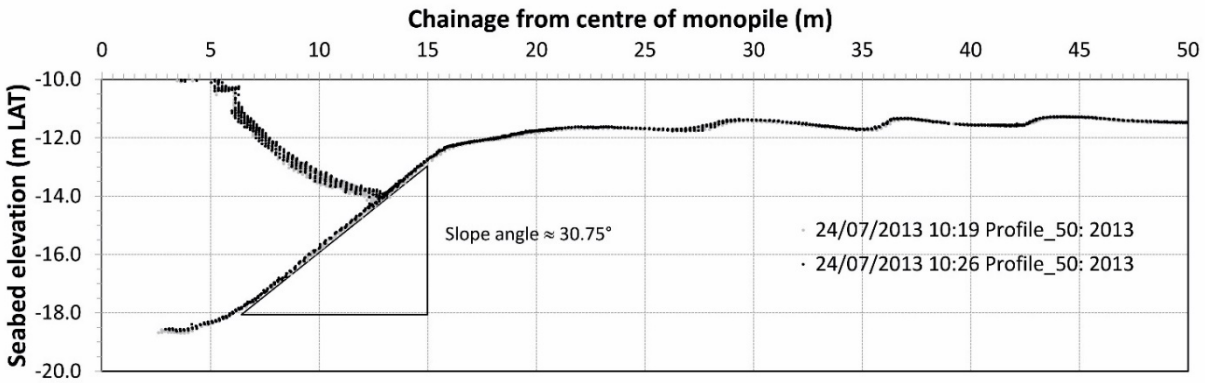

(c)

Figure 9: Cross-sectional profiles along the flow and cable axis (50° alignment anticlockwise from east).

Continued

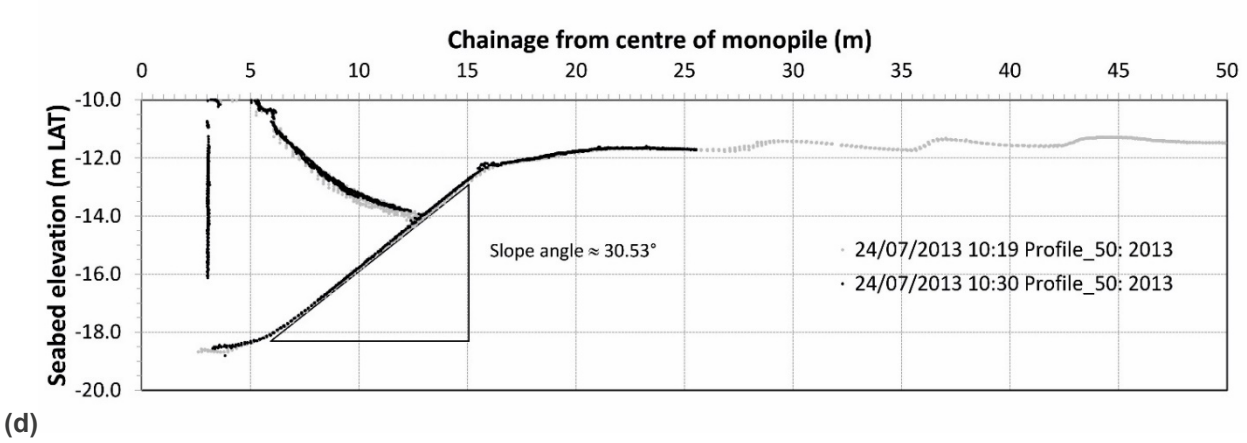

(d)

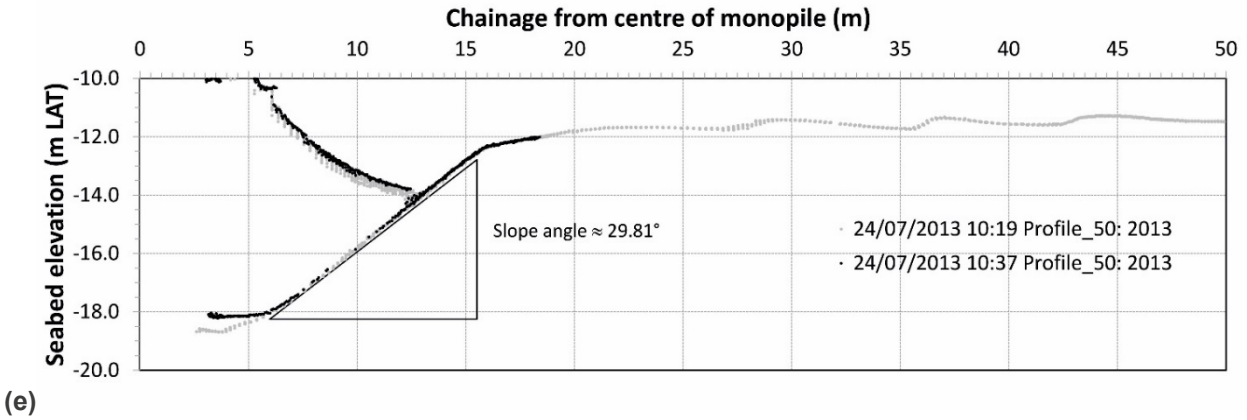

(e)

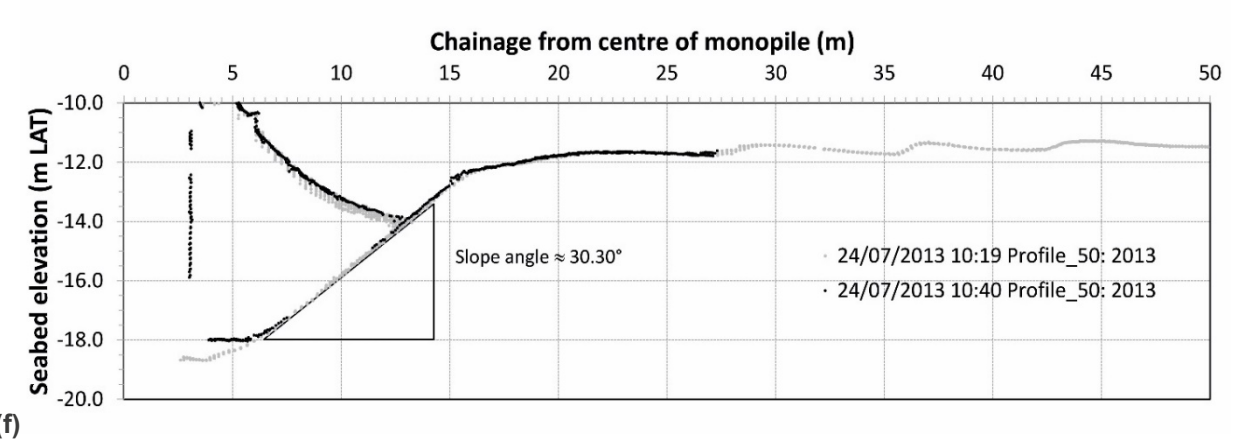

(f)

Figure 9: Cross-sectional profiles along the flow and cable axis (50° alignment anticlockwise from east).

Continued

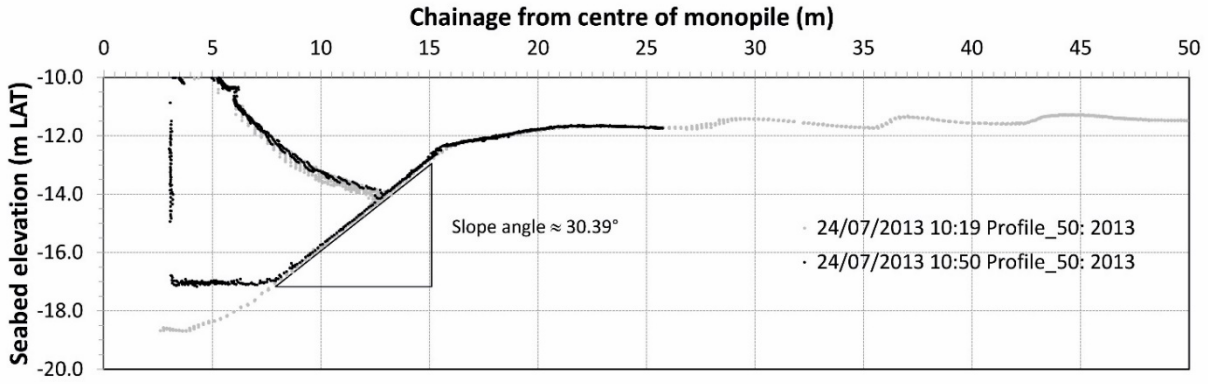

(g)

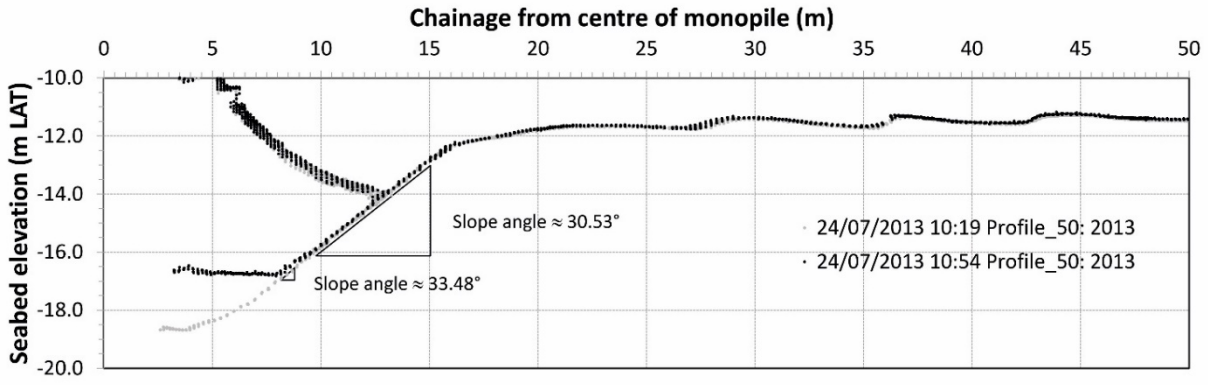

(h)

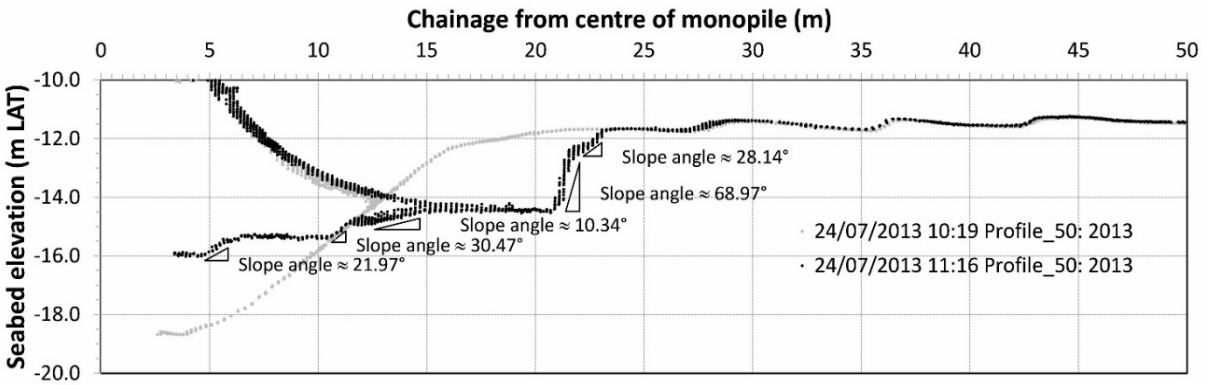

(i)

Figure 9: Cross-sectional profiles along the flow and cable axis (50° alignment anticlockwise from east).

Continued

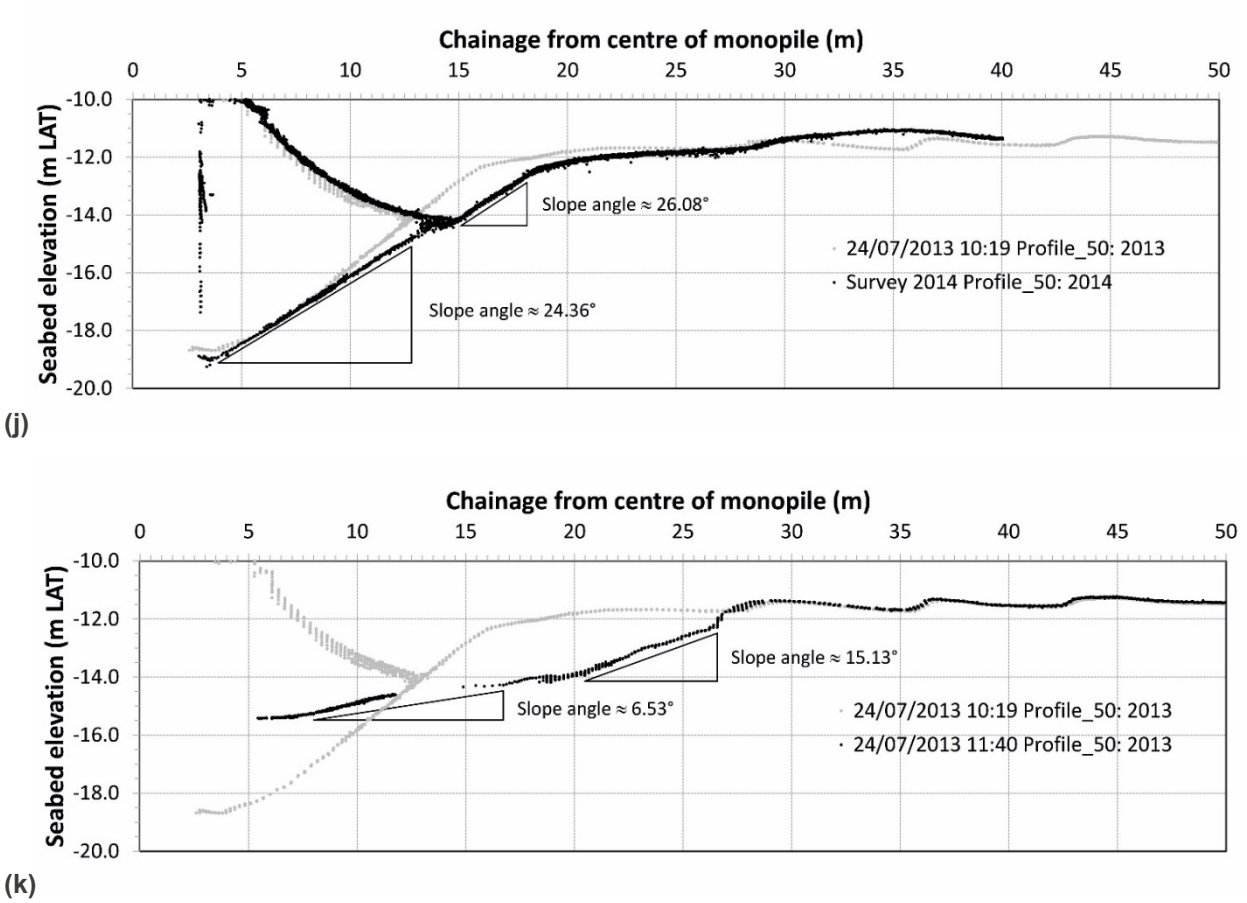

Figure 9: Cross-sectional profiles along the flow and cable axis (50° alignment anticlockwise from east).

From the cross-sectional profiles presented in Figure 8 corresponding to an alignment of 20° anticlockwise from east, the start of the collapse can be observed in Figure 8c. At a chainage of about 7 m from the centre of the monopile a small depression in the slope is observed and some material has begun to deposit in the base of the scour hole. In Figures 8d and 8e the loss of soil has continued and takes the form of an arc, similar to the classical slip circle form. These changes have occurred within about 11 minutes. About, three minutes later the form of the arc has begun to steepen at the upper face (Figure 8f). Whilst the position of the back face remains at about 14 m from the centre of the monopile between 10:37 and 10:40 (Figures 8e and 8f) material lower down the slope is being lost to the base of the scour hole. By 10:50 (Figure 8g - about 10 minutes later) the back face has moved outwards by about 4.4 m and the material is infilling the base of the scour hole with a difference of about 0.9 m (shallower) between 10:40 and 10:50.

By 10:54 (Figure 8h) the back face of the slip surface is showing instability around mid-position and 22 mins later (Figure 8i) the slope has collapsed moving back a further 7 m and infilling the base of the scour hole by a further 1.7 m. The final cross-section from the slip event is at 11:40 am (Figure 8j) about 75 mins from the start of the collapse. The back face of the slip has moved a further 1.7 m from the position shown in Figure 8i and the scour hole has shallowed, on average, by a further 0.6 m.

Figure 9 shows the corresponding cross-sections along the principal tidal flow axis. Changes in slope are not observable until about 11:16 (Figure 9i) although infilling of the base of the scour hole can be observed from about 10:37 (Figure 9e).

In addition to Figure 9 showing the cross-sections along the principal tidal flow axis they also correspond to the alignment of one of the inter-array cables. This is of interest due to the recorded post-cable installation seabed profile after the cable was jetted into the seabed. Figure 10 shows the pre-cable burial seabed profile together with the corresponding profile from the December 2012 survey. The two profiles show similar undisturbed seabed levels, although the earlier pre-cable burial survey shows slightly smaller scour hole extents and reduced magnitude of scour.

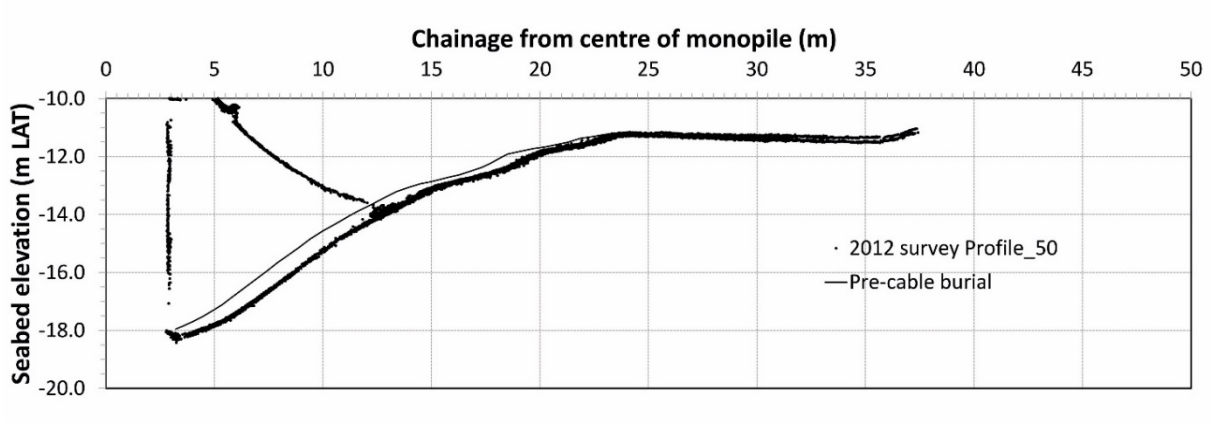

Figure 10: Cross-sectional profiles along a 50° alignment anti-clockwise from east showing pre-cable burial seabed profile together with the corresponding December 2012 profile.

Figure 11 shows the post-cable burial seabed profile together with corresponding pre- and post-collapse profiles. The approximate cable catenaries are also shown. Of particular interest is the close similarity in levels between the post-cable burial and the post-collapse profile. Whilst the back face of the scour hole collapse profile extends further from the centre of the monopile the overall similarity is striking and does raise the question of whether the final scour hole collapse profile was influenced by the jetting process used at cable installation. However, it is of note the initial slope failure did not occur along the alignment of the cable, although it is possible that the jetting formed a preferential slip plane for the failure.

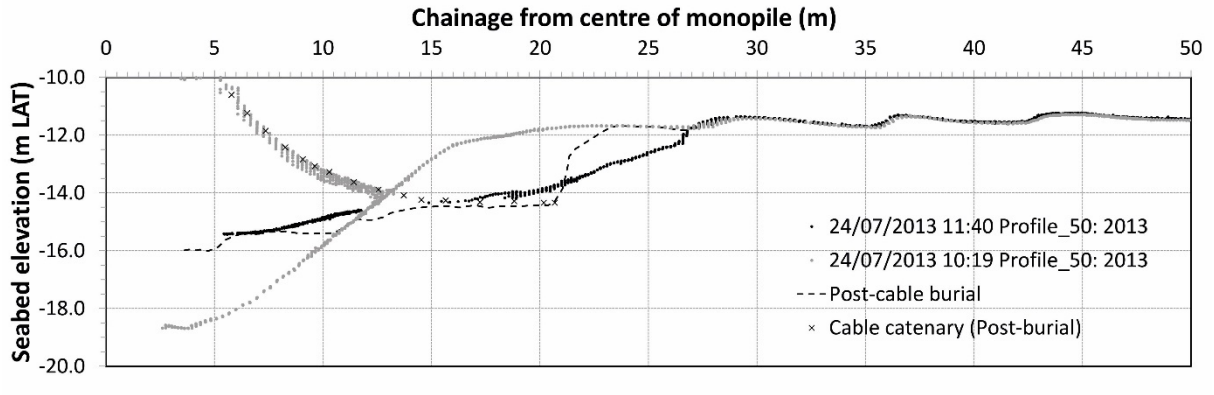

Figure 11: Cross-sectional profiles along a 50° alignment anti-clockwise from east showing post-cable burial seabed profile together with the pre- and post-collapse profiles. The approximate cable catenaries are also shown.

As mentioned above the lateral flow of sediment in the scour hole is observed in the filling up of the scour hole in Figure 9e and following (i.e. 10:37 onwards). It is noted that the filling soil material does generate sediment deposition on the opposite side of the pile. By 10:54 the material may have already flowed around the pile but the data is not clear in this region close to the pile, and has definitely reached the opposite side of the pile by 11:16. At a distance of 3.5 to 5 m from the centre of the monopile on the opposite side to the monopile the bed elevation is around -16 m, i.e. about 2 m higher than the pre-collapse scour hole at this location and about 1 m lower than the post-collapse levels on the failure side. By the time of the 2014 survey this material has been scoured out as shown in Figures 7a and 7b.

6. Discussion

A significant amount of research has been published on submarine slope failures, however, the size of these failures is generally on the scale of hundreds of metres or, in the case of the Storegga slide in the North Sea, hundreds of kilometres. Slope failures are common on inclined areas of the seabed, predominantly in locations with weak sedimentary materials or fractured rock that are subject to significant environmental stresses such as earthquakes, large storm waves, and high internal pore pressures (Hampton *et al*., 1996). Submarine landslides can involve the movement of significant volumes of material (for example the Storegga slide resulted in the movement of about 3,500 km^3 of material) or slope failure in the Westerschelde (1 million m^3 of material) (Mastbergen, *et al*., 2016). In the present study, the slope failure is at a comparatively small scale (tens of metres) when considered alongside these larger scale submarine slides. In addition, the slope failure is associated with the presence of a monopile foundation, which further complicates the local flow behaviour and soil response.

Terzaghi (1957) noted that the slope angle of a non-cohesive soil is equal, in its limit, to the critical state friction angle, φ_{cr}, but in nature the observed slope angle of submarine slopes is generally shallower due to the action of external agents (hydrodynamic or seismic). However, active scour holes around foundations are maintained in a state of instability by the balance between the hydrodynamic forces acting on the seabed and the structure, the structural response with respect to the soil-structure-fluid interaction and the geotechnical properties of the soil. In its limit this state is a form of dynamic equilibrium.

6.1. Scour as a conditioning ground geometry and a trigger

Whilst it is not the intention to provide a detailed description of the scour process, an overview is required, as reference will be made to both the mechanisms driving the scour process and those related to geotechnical slope failure later within the discussion.

The flow pattern near a pile or pier is quite complex and has been investigated by numerous researchers, for example, Breusers and Raudkivi (1991) and Melville and Coleman (2000). The principal features of scour around a circular pile are well defined: the downflow at the upstream face of the pile; the horseshoe vortex at the base of the pile; a surface roller (or bow wave) at the upstream face of the pile; and wake vortices downstream of the pile (Figure 12).

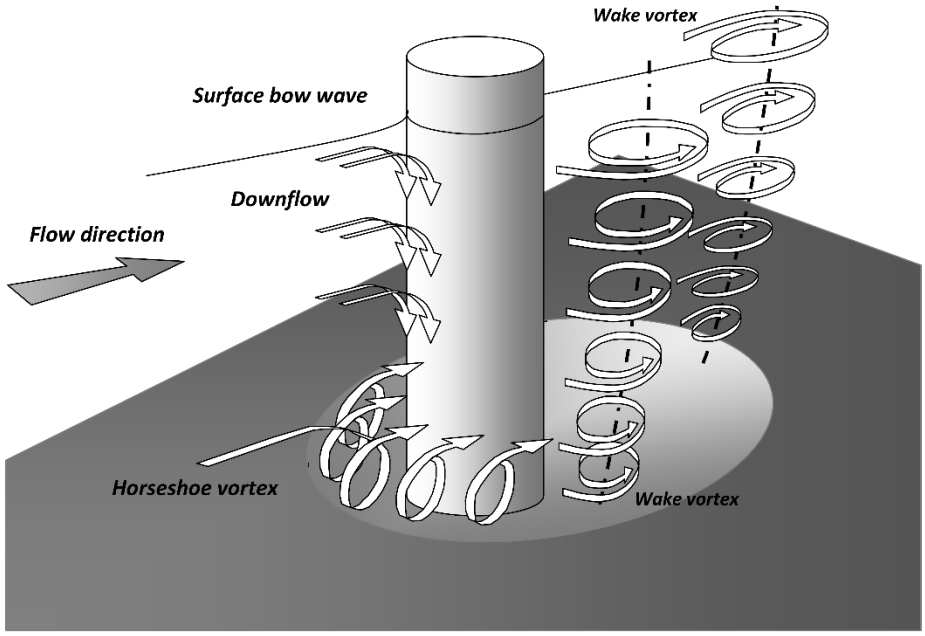

Figure 12: Schematic showing scour process under an unidirectional current. (After Melville and Coleman, 2000).

The downflow is a result of flow deceleration in front of the pile. The associated stagnation pressures on the face of the pile are greatest near the water surface, where the deceleration is largest, and decrease downwards. This resulting downwards pressure gradient at the face of the pile leads to the downflow, which impinges on the bed, acting like a vertical jet and eroding a groove immediately adjacent to the pile face. The creation of the groove undermines the scour hole slope above and this slope then collapses bringing sediment into the erosion zone. The development of the scour hole around the pile creates a lee eddy, known as the horseshoe vortex. The horseshoe vortex develops as a result of flow separation under the influence of the adverse pressure gradient induced by the presence of the structure itself. The horseshoe vortex is effective at transporting sediment away from the scour hole. Therefore, the downflow and horseshoe vortex are the primary mechanisms in the scour hole development. Petersen (2014), Petersen *et al*. (2015) and Baykal *et al*. (2015), for example, also mention the effect of large-scale counter-rotating streamwise vortices in the lee-wake on scour development.

The wake vortices are a consequence of flow separation at the sides of the pile. These vortices travel downstream due to the mean flow. Breusers and Raudkivi (1991) describe these cast-off vortices as having vertical low pressure centres lifting sediment from the bed like miniature tornados, whilst Melville and Coleman (2000) describe the vortices as acting like vacuum cleaners sucking sediment from the bed as well as transporting sediment entrained by the downflow and horseshoe vortex.

Along with the sediment lifting and transportation, the effects that the horseshoe vortices and the wake vortices have on the soil surrounding the pile will translate into a decrease in the pore pressure of the soil mass directly below the scoured area, corresponding to the toe of the established slope.

Under tidal conditions the time-varying current reverses direction with the tidal phase, consequently the scour development will take place in two directions. In addition, the magnitude of the current will vary through the period of the spring-neap tidal cycle (see Figure 3b).

From the numerical model, the start of the slope failure occurs towards the end of the flood tide as shown in Figure 13 as the tidal current is reducing. Therefore, during tidal flow the upstream scour slope will be subject to the lift forces associated with the horseshoe vortices formed around the monopile in the scour hole which reduce in strength with the reducing tidal velocity towards high water. Therefore, there will be a decaying lift force acting on the sediment in this latter period of the tide.

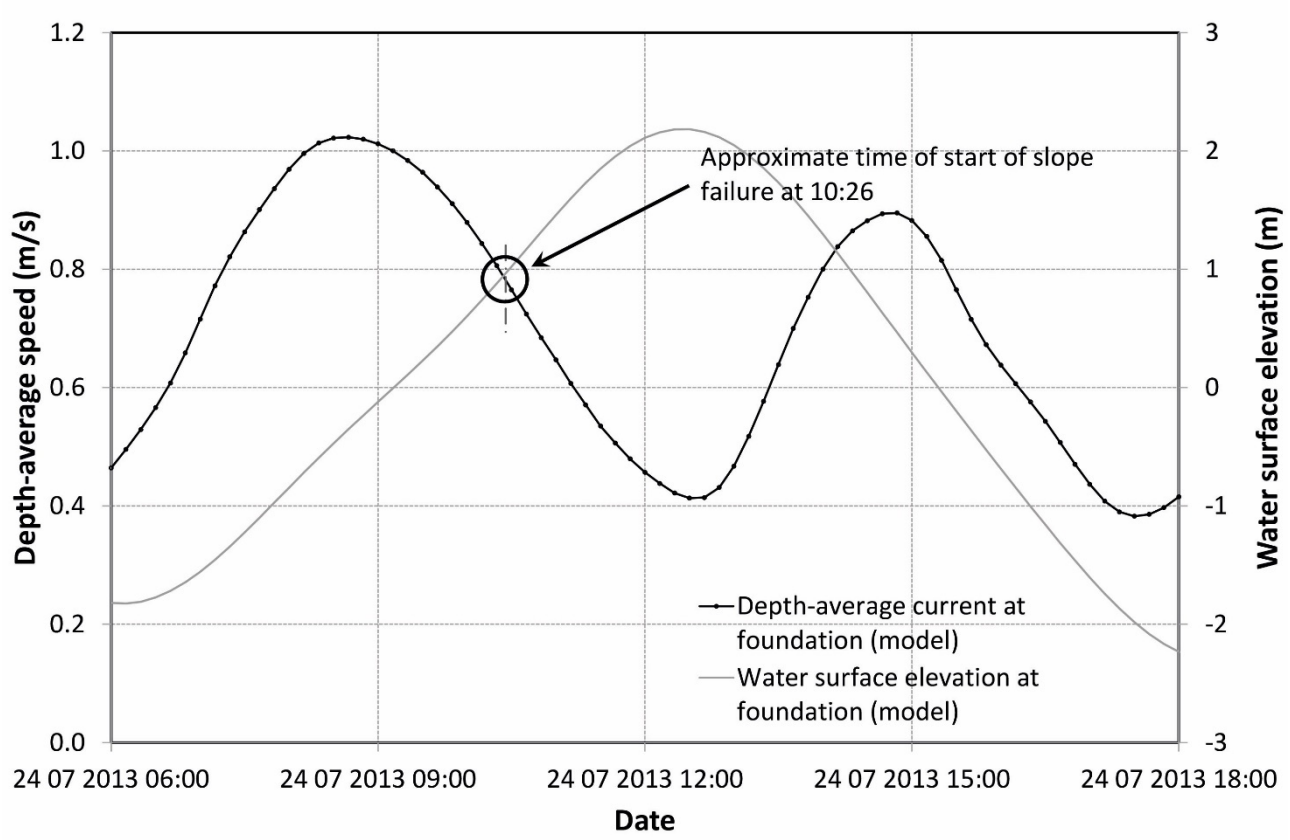

Figure 13: Approximate start of the slope failure relative to the modelled tidal current and water surface elevation.

In general, submarine slope instabilities can be caused by a number of possible failure mechanisms including: the deposition of sediment causing increased overburden on a steep slope that exceeds the bearing capacity of the soil, i.e. gravitational forces in weak soils; seismic action; gas hydrate dissociation; and, hydraulic forcing such as that due to currents, waves, tides, (or combinations of), pore water pressure differences leading to liquefaction or movement of sediments. In the present case, the information available for the observed slope failure is derived from the multi-beam images, metocean data collected in the region, numerical simulation of the tidal hydrodynamics and geotechnical information available prior to installation of the monopile.

With respect to seismic action, this can be ignored as a possible trigger in the present case. There are also no gas hydrates present in the study area. However, in the case of structures placed offshore, they are subject to wind, wave and current loading. Further, with respect to offshore wind, the operation of the turbine will induce dynamic loading within the pile. It is possible that over time this cyclic loading may trigger a

response in the local seabed soils although very few studies have been published on this potential mechanism (Reese *et al*., 1989; Al-Hammadi and Simons, 2016). The corresponding movement of the pile in response to loading being dependent on the resultant soil reaction.

The gravitational force provides a mechanism for general downslope movement of the sediment particles as well as sediment consolidation. Wave loading on seabed sediment induces stresses that are transient, with each peak lasting for perhaps a fraction of a second to several seconds. Therefore, the sediment response to this transient loading will be different than that due to a sustained load. For example under this transitory loading the sediment response may be a progressive loss of strength leading to liquefaction and movement of the sediment under its own weight. However, from the wave measurements collected at the time of the collapse a wave-induced slope failure can be ruled out.

It is not clear if the monopile foundation could have added to the scour mechanism. Since the foundation structure is being subjected to a range of operational cyclical loadings (wind and wave actions), the rocking motion could help in the compaction of the soil.

Al-Hammadi and Simons (2016) noted from experiments that vibration of the pile can reduce local scour depth through the cascade of sand particles into the scour hole, whilst the presence of vibration at the start of the scour process has the potential to increase the depth of scour significantly. However, with the presence of currents, there is a strong possibility that the agitated material is also being dragged along with the seabed sediments, further widening the gap between the pile and the soil, as well as increasing the depth of the scour.

Chu *et al*. (2002) suggested that scour at the toe of the slope, especially for dense granular soil slopes, may be an important factor for stability. Based on the present data of the existing ground conditions and of the involved scour mechanisms, it is reasonable to state that the slope prior to failure is considered to be unstable.

The source of this instability sits within the fragile equilibrium between the scour vortices, which move the seabed material along the scour slopes, at different stages and with different levels of effect. As mentioned, a natural slope will find stability in a geometry that respects its internal properties, namely cohesion and angle of shearing resistance. With the presence of the scour hole inducing an upwards flow, responsible for sediment transportation and the alteration of the established pore pressure in the soil, the toe of the slope will have a significant degradation of its soil matrix.

6.2. Slope failure process

One slope failure mechanism observed as a production mechanism for offshore dredging (Breusers, 1974; van Rhee and Bezuijen, 1998) is termed breaching. Mastbergen *et al*. (2016) observed flow slides in the Westerschelde where they were created at a test site by dredging to steepen the toe of the slope of the estuary channel. As mentioned earlier, the site had experienced a large flow slide previously with almost 1 million m^3 of material. The test site had a generally uniform fine sand with d_{50} about 0.14 mm and d_{60}/d_{10} about 1.5, where d_{10} and d_{60} are the 10 and 60 percentile sizes. Small retrogressive breaches were generated with active breach heights of 6 m and recession speeds of between 10 and 20 metres per hour (0.0028 to 0.0055 m/s).

This type of failure can occur in densely packed soils. The trigger mechanism for this phenomenon are negative pore pressures within the soil (van Rhee, 2015), which in the case of dredging operations are caused by the inflow of the suction tube of dredgers (i.e. the tube sucks water out of the sediment pack) but in the case of offshore wind turbines may be caused by the near-bed horseshoe vortex and the large-scale

counter-rotating streamwise phase-averaged vortices (LSCSVs), which effectively cause an upwards flow, and which can have the same effect on the sediment as the suction from the dredger. LSCSVs are mainly driven by the longitudinal counter-rotating vortices which are created partly by the horseshoe vortex and the variation of the shedding frequency over the height of the structure (Baykal et al., 2015). These negative pore water pressures give a temporary strength to the soil which manifests into high angles of repose (up to 90 degrees). These steep underwater slopes radiate away from the initial point of disturbance and create a sediment flow towards the lower part of the scour hole.

The slope failure process described in the previous sections shows evidence that it may be linked to the breaching process. But to this day, breaching has never been identified as a potential threat for offshore foundations. To confirm this hypothesis (i.e. that the slope failure observed in this paper is caused by breaching) the van Rhee (2015) model has been implemented to calculate wall velocity (v_w), which is the velocity at which the steep soil slope moves away from the point of origin of the disturbance. The formulation is given as:

$$i_{eq} = 0.0049 s^{-0.39} d_{50}^{0.92} \quad (1)$$

where i_{eq} is the equilibrium slope angle; d_{50} is the median sediment diameter. Here s is the sediment flux and can be determined as:

$$s = \rho_s (1 - n_0) H v_w \quad (2)$$

With ρ_s the sediment density; n_0 the porosity of the soil; H the height of the soil wall (steep slope); and v_w the velocity at which the soil wall moves away from the point of origin of the disturbance.

This model is compared with the analysis of profile data which yields information for the time evolution of the soil profile during the event.

The evolution of the sediment levels along the scour pit in the axis of the failure were extracted from the bed profiles and plotted in Figure 14a. This shows the bed elevation at 30 m is not affected by the collapse whereas the most change leading to infilling of the scour hole is experienced 3.5 and 5 m from the pile centre in the bottom of the scour hole.

The recession distance is plotted with time in Figure 14b. Initially the edge of the scour hole is not affected by the slope failure and remains constant at about 14 m from the pile wall. By about 2000 seconds the scarp of the failure has reached the edge of the scour hole and the scour hole grows in length as it is captured by the slope failure.

The data for scarp and toe distance in Figure 14 (b) yields the interpreted ‘average’ retreat rate from the toe and scarp of the failure along the 20 degree alignment plotted in Figure 15. The data show an average recession rate of 0.0049 m/s in the growth phase (to 3420 seconds) and 0.0013 m/s in the relaxation phase beyond 3420 seconds.

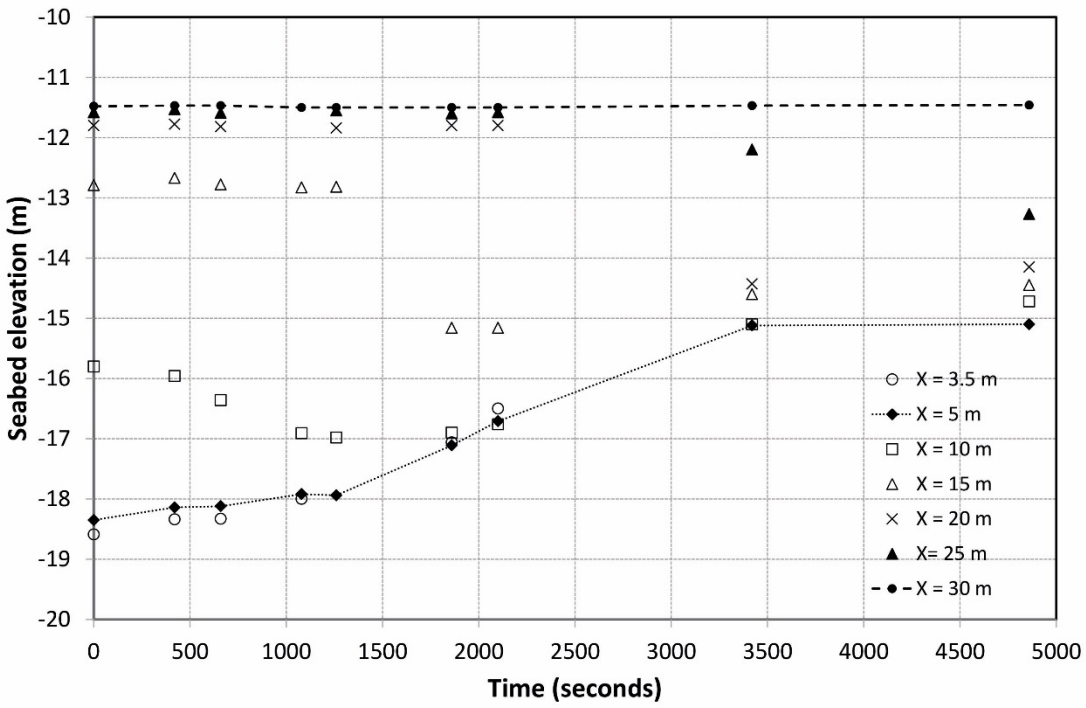

(a)

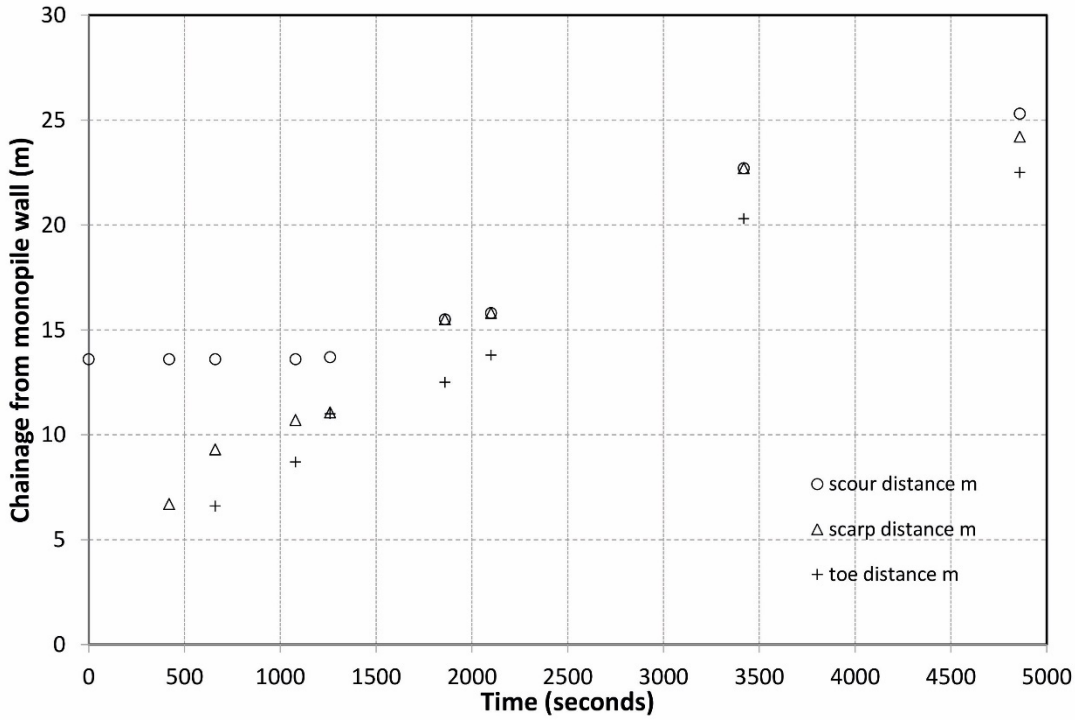

(b)

Figure 14: (a) Elevation changes with time for selected distances X from the monopile centre and (b) recession distance from the monopile wall compared to the pre-event distance to the edge of the scour hole.

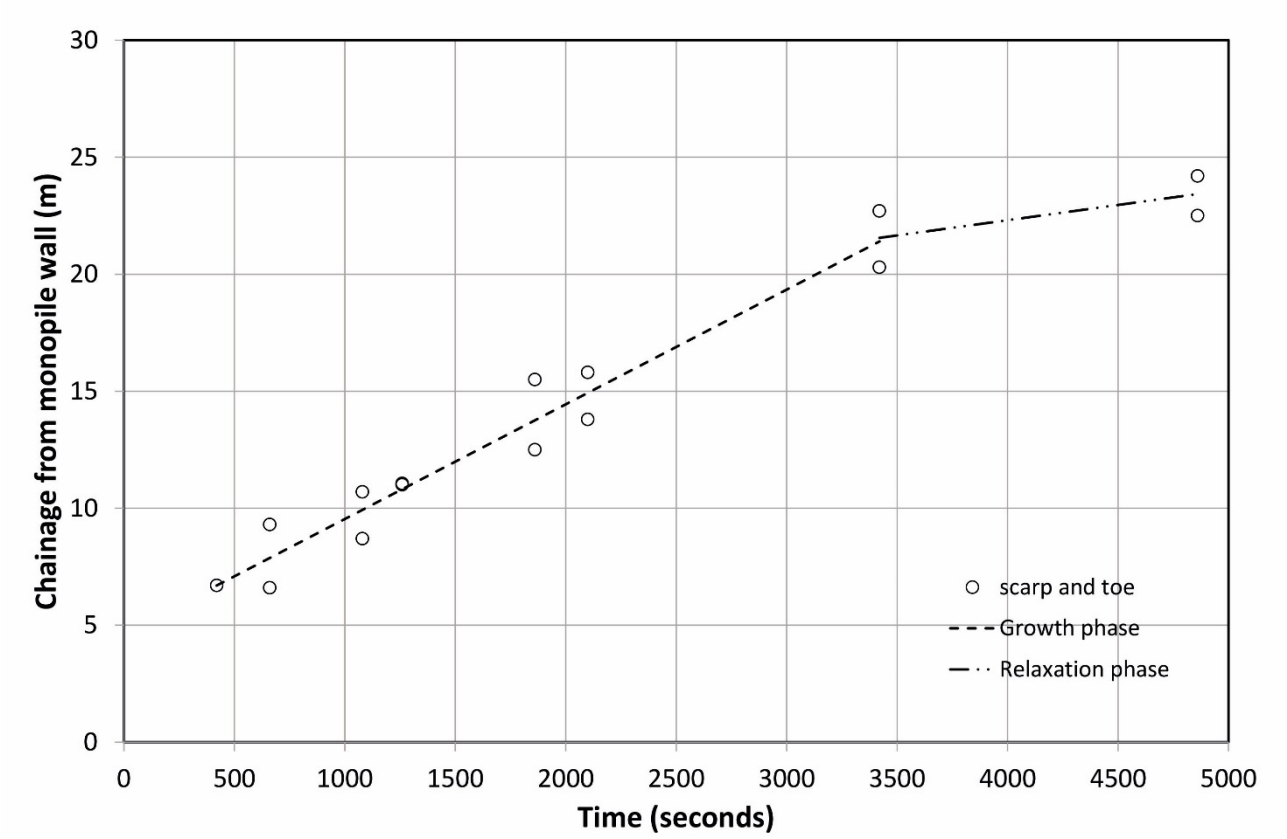

Figure 15: Slope recession with time yielding linear average values.

Figure 16 shows a comparison between the wall recession velocity as a function of the sediment size calculated using van Rhee (2015) and the measured wall velocity which was determined from Figure 8 for the cross-sectional profiles along the 20° alignment. Here v_w is calculated using the geotechnical information presented earlier. Comparing the measured and calculated wall velocity it can be observed that the two lines intersect within the range of d_{50} found on the site. This demonstrates the breaching model has the capability of predicting the rate at which the slope failure takes place. The fact that the recession rates in Figure 16 lie within the limits predicted by the model support the assessment that breaching is the most probable cause of the scour hole collapse.

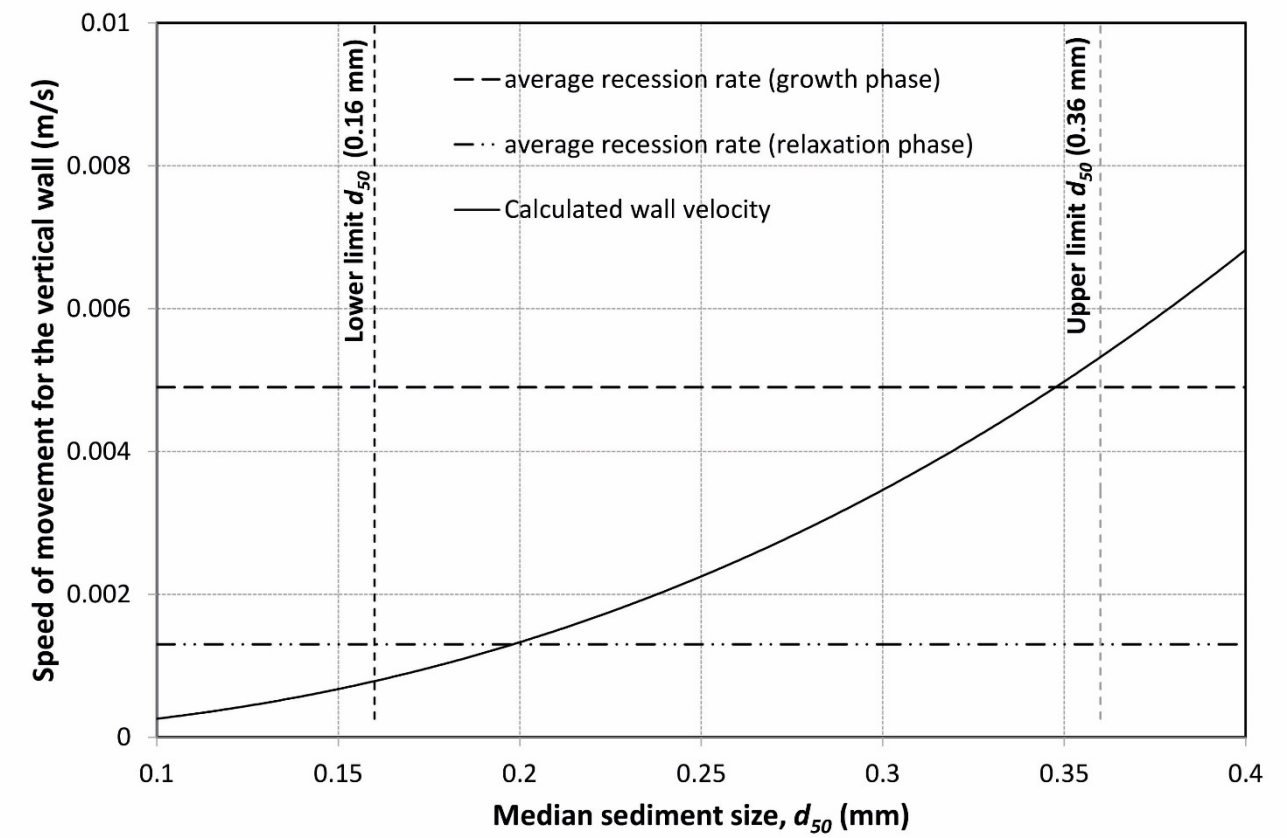

Figure 16: Comparison between Breaching model prediction measured value of the wall speed with upper and lower limits of d50 for site shown.

6.3. Screening of soil susceptibility

The remaining step in the investigation is to screen the CPTU data for the soil column to the depth of the local scour hole in terms of the Soil Behavior Type chart of Robertson (2010). The results for cone resistance q_c and friction ratio Fr equate to dense sand and possibly gravel. The normalized values plotted in Figure 17 show predominantly sand mixtures (silty sand and sandy silt). OCR in the figure is the over-consolidation ratio, and is defined as the maximum value of effective stress in the past divided by the present value. Since both the penetration resistance and sleeve resistance increase with depth due to the increase in effective overburden stress, the CPTU data requires normalization for overburden stress for very shallow and/or very deep soundings. Robertson's (2010) analysis of flow liquefaction case histories show the soil data for those cases plot below the $Q_{tn,cs} = 70$ line. The CPTU data for the monopile location are plotted on Figure 17 and lie below this line, and hence the soil is classified for screening purposes as contractive and in the A_2 zone (Robertson, 2010, Figure 8) in which flow liquefaction is possible depending on loading and ground geometry.

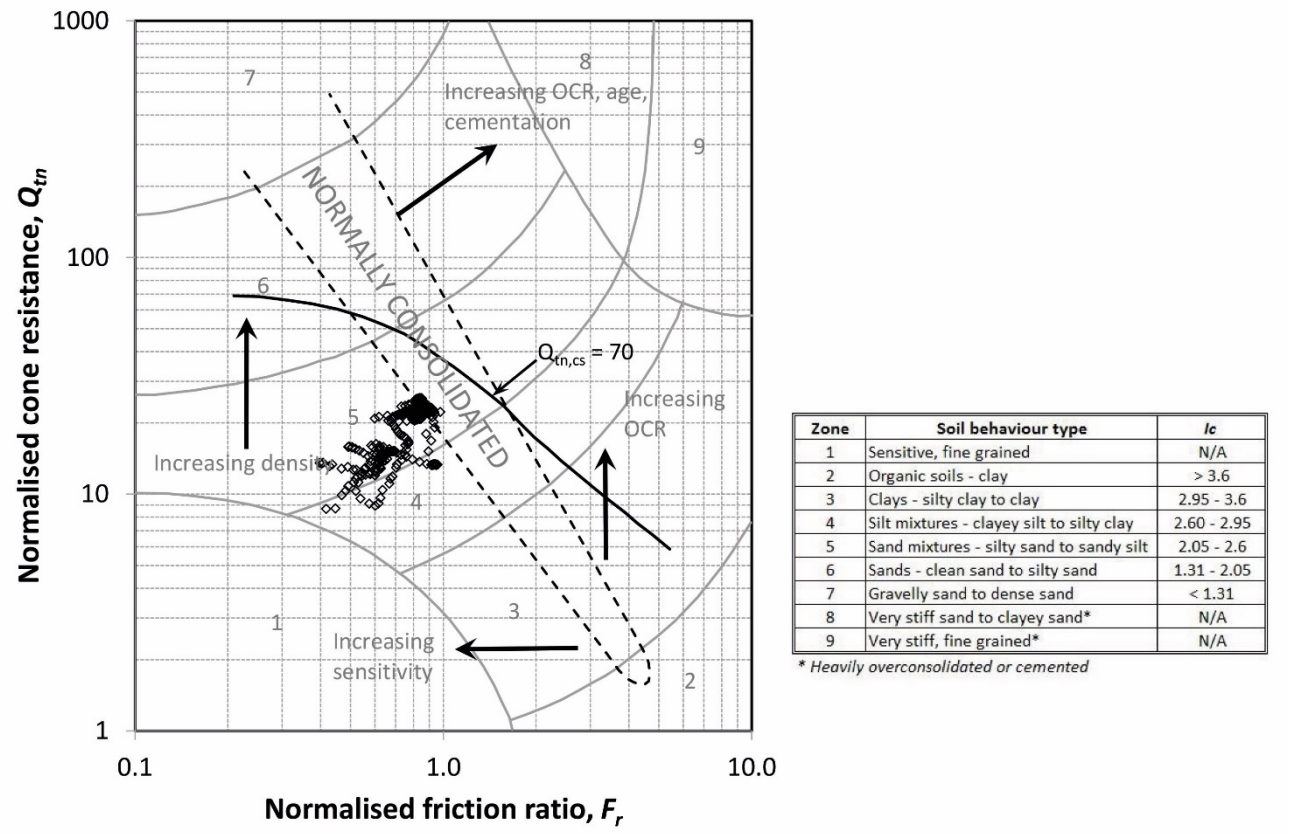

Zone	Soil behaviour type	*Ic*
1	Sensitive, fine grained	N/A
2	Organic soils - clay	> 3.6
3	Clays - silty clay to clay	2.95 - 3.6
4	Silt mixtures - clayey silt to silty clay	2.60 - 2.95
5	Sand mixtures - silty sand to sandy silt	2.05 - 2.6
6	Sands - clean sand to silty sand	1.31 - 2.05
7	Gravelly sand to dense sand	< 1.31
8	Very stiff sand to clayey sand*	N/A
9	Very stiff, fine grained*	N/A

** Heavily overconsolidated or cemented*

Figure 17: Normalized CPTU parameters for site plotted on Robertson (2010) axes for screening flow liquefaction for the equivalent clean sand resistance, Qtn,cs ≤ 70.

The lack of confining lateral pressure due to the void caused by the presence of the scour hole, combined with the oversteepening of the scour hole and pressure field reduction in the scour hole as flow strength around the monopile reduces in the last portion of the flood tide, are consistent with triggering of the collapse event.

As such, for the case in hand, a succession of slides and slope rearrangements took place. Starting from the initial geometry of an approximately 30° slope angle scour hole with a height of 7.0 m (Figure 8b) a series of slides, caused by the removal of material along the slope, progressively rearranged the slope geometry. This rearrangement propagated away from the monopile and upwards until it reached the existing seabed level. Comparing the initial section with the one 8 months after the event was recorded, as shown in Figure 8k, the final impact of the rearrangement is a small deepening around the pile (approximately 1.0 m) and the smoothing of the crest of the scour hole (it retracted 6.0 m).

Despite the differences in geometry some months prior to and some months after the event not being too great, the evolution of the collapse process itself over 75 minutes showed some phases where the additional void created was fairly large (Figure 8g-8i).

6.4. Appreciation of similarities elsewhere and implications

A further question is whether the captured slope failure at the monopile presented above is an one-off event or something that is more commonly occurring across the site. Again, by chance as part of routine operations multi-beam survey images of similar slope failures have been captured at other turbine foundation locations (Figure 18).

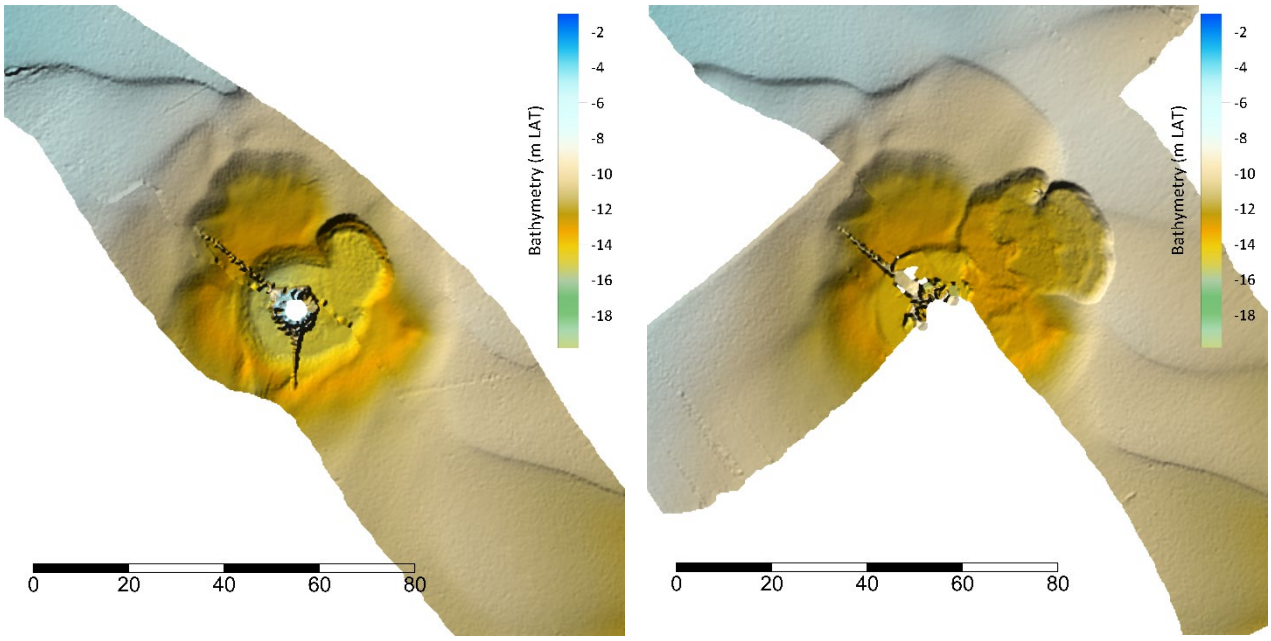

Figure 18: Slope failure at another monopile location at two instants in time.

The other related question is whether these type of failure events are continually occurring at these locations. Evidence is required from wind farm sites within morphologically active seabed regions where continuous monitoring is taking place to determine the frequency and magnitude of these type of events. Further, from Figure 18 the image suggests that a slope failure has occurred previously at this foundation albeit along a different failure plane. Given that the scour holes are in a continual state of instability, it is more than likely that these failure events reoccur, although the frequency of occurrence will be much more difficult to predict since the triggering mechanisms may vary depending on the prevailing metocean conditions at the time. We anticipate that the trigger mechanisms will relate to increased scouring potential on large tidal ranges (this collapse event occurred during spring tides, Figure 3b) and surcharging of the edge of the scour hole by sediment transport. If the sediment transport rate is low then the collapse areas will only infill very slowly and hence further collapses along the same axis are not anticipated until infill has taken place as the slope will have relaxed.

The implications of slope collapses in scour holes are as follows:

- the scour hole depth and extent surveyed after a collapse may look shallower and longer, respectively, than during dynamically stable periods of scouring;
- the volume of the (lower portion of the) scour pit will be temporarily reduced and if scour protection was being installed at this time the volume would be reduced to achieve the target level of fill;

- the scour hole shape will look irregular and experience periodic lowering which may expose buried cables locally to the scour pit. The displaced soil may flow against exposed cables in the scour hole as a lateral load; and,
- the bearing capacity of the soil adjacent to the scour pit may be locally reduced, which has implications for seabed interventions and jack-up operations.

7. Conclusions

The unique multi-beam survey dataset presented within this paper provides evidence of a geotechnical slope failure in a naturally formed scour hole at an offshore wind turbine monopile foundation. The data captures the failure event over a period of about 75 mins over which time about 450 m^3 of material is moved.

The observed scour around the monopile is not unusual for the given flow and seabed conditions, however, the collapse of the slope to the authors' knowledge has not been observed previously.

The level of available information at the location of the observed slope failure make it difficult to determine the exact trigger of the slip. However, given the various mechanisms acting at the pile (hydrodynamic, geotechnical and structural) a slip event, through the process of breaching, could perhaps be anticipated for the reasons discussed above.

Such slip events may provide a mechanism for the gradual expansion of scour holes over time in sites consisting of relatively uniform non-cohesive sand sediments. In addition, the growth in scour hole volume may also lead to a gradual increase in scour depth over time.

From the evidence presented it is anticipated that such events are expected to be relatively common in active scour environments with sandy soils.

8. Acknowledgements

This research was funded by HR Wallingford Ltd.'s scour research programme and was partly undertaken while the lead author was a Visiting Research Fellow in the School of Civil, Environmental and Mining Engineering within the Faculty of Engineering, Computing and Mathematics at the University of Western Australia.

9. References

Al-Hammadi, M. and Simons, R.R. (2016). Effect of vibration on the scour process around cylindrical structures under unidirectional flow in a sandy bed. In: *Scour and Erosion. Proc. 8th Int. Conf. on Scour and Erosion*, Oxford, UK, 12 – 15 September, (eds.) Harris, J., Whitehouse, R. and Moxon, S., CRC Press, p. 157 – 161.

Baykal, C., Fuhrman, D.R., Sumer, B.M., Jacobsen, N.G. and Fredsøe, J. (2015). Numerical investigation of flow and scour around a vertical circular cylinder. *Philos. Trans. R. Soc. A*, 373: 20140104.

Breusers, H.N.C. (1974). Suction of sand. *Bulletin of International Society of Engineering Geology*, 10: 65–66.

Breusers, H.N.C. and Raudkivi, A.J. (1991). *Scouring*. IAHR Hydraulic Structures Design Manual, 2, A. A. Balkema, Rotterdam, vii + 143 pp.

Chu, J., Ho, M.G., Loke, W.L. and Leong, W.K. (2004). Effects of scour and hydraulic gradient on the stability of granular soil slope. *Proceedings of Second International Conference on Scour and Erosion*, Singapore, 16-17 November 2004. Vol 2, 439-452.

Hampton, M.A., Lee, H.J., Locat, J. (1996). Submarine landslides. *Reviews of Geophysics*, 34, p. 33 - 59. doi: 10.1029/95RG03287.

Harris, J.M., Whitehouse, R.J.S. and Benson, T. (2010). The time evolution of scour around off-shore structures. *Proceedings of the Institution of Civil Engineers, Maritime Engineering*, 163, March, Issue MA1, pp. 3 – 17.

Mastbergen, D., van den Ham, G., Cartigny, M., Koelewijn, A., de Kleine, M., Clare, M., Hizzett, J., Azpiroz, M. and Vellinga, A., (2016). Multiple flow slide experiment in the Westerschelde Estuary, The Netherlands. Chapter 24 in Submarine Mass Movements and their Consequences, G. Lamarche et al. (eds), *Advances in Natural and Technological Hazards Research*, 41, 241-249.

Melville, B.W. and Coleman, S.E. (2000). *Bridge Scour*. Water Resources Publications, LLC, Colorado, USA, 550 p.

Petersen, T.U. (2014). *Scour around offshore wind turbine foundations*. PhD thesis, Section for Fluid Mechanics, Coastal and Maritime Engng., Dept. of Mechanical Engng., Technical University of Denmark, Lyngby.

Petersen, T.U., Sumer, B.M., Fredsøe, J., Raaijmakers, T. and Schouten, J. (2015): Edge scour at scour protection around piles in the marine environment - Laboratory and field Investigation. *Coastal Engineering*, December, 106 (2015) 42-72.

Reese, L.C., Wang, S.T. and Long, J.H. (1989). Scour from cyclic lateral loading of piles. In: *Proceedings 21st Offshore Technology Conference*, Paper OTC 6005, Houston, Texas, 1 – 4 May, pp. 395 – 402.

Robertson, P.K. (2010). Evaluation of flow liquefaction and liquefied strength using the cone penetration test. *Journal of Geotechnical and Geoenvironmental Engineering*, Vol. 136, No. 6, June, p. 842-853.

Soulsby, R.L. (1997). *Dynamics of marine sands: A manual for practical applications*. Thomas Telford Publications, London, 249 pp.

Sumer, B.M. and Fredsøe, J. (2002). *The Mechanics of Scour in the Marine Environment*. Advanced Series on Ocean Engng., Vol. 17, World Scientific, Singapore. xiii + 536 pp.

Sumer, B.M., Petersen, T.U., Locatelli, L., Fredsøe, J., Musumeci, R.E. and Foti, E. (2013). Backfilling of a scour hole around a pile in waves and current. *J. of Waterway, Port, Coastal, and Ocean Engng.*, Vol. 139, No. 1, January 1, pp. 9 -23.

Terzaghi K. (1957). *Varieties of submarine slope failures*. Norwegian Geotechnical Institute, Publication N. 25, p. 1 - 16.

van Rhee, C. (2015). Slope failure by unstable breaching. *Proceedings of the Institution of Civil Engineers Maritime Engineering*, 168, June, Issue MA2, p. 84–92.

van Rhee, C. and Bezuijen, A. (1998). The breaching of sand investigated in large-scale model tests. In: *Coastal Engineering 1998* (Edge BL (ed.)). American Society of Civil Engineers, Reston, VA, USA, vol. 3 pp. 2509–2519.

Whitehouse, R.J.S. (1998). *Scour at marine structures: A manual for practical applications*. Thomas Telford, London, 198 p.